Original article

MOLECULAR METABOLISM

Tanycytes release glucose using the glucose-6-phosphatase system during hypoglycemia to control hypothalamic energy balance

María José Barahona[1,2,3], Luciano Ferrada[2], Matías Vera[1,2], Francisco Nualart[1,2,*]

ABSTRACT

Objective: The liver releases glucose into the blood using the glucose-6-phosphatase (G6Pase) system, a multiprotein complex located in the endoplasmic reticulum (ER). Here, we show for the first time that the G6Pase system is also expressed in hypothalamic tanycytes, and it is required to regulate energy balance.

Methods: Using automatized qRT-PCR and immunohistochemical analyses, we evaluated the expression of the G6Pase system. Fluorescent glucose analogue (2-NBDG) uptake was evaluated by 4D live-cell microscopy. Glucose release was tested using a glucose detection kit and high-content live-cell analysis instrument, Incucyte s3. *In vivo G6pt* knockdown in tanycytes was performed by AAV_1-shG6PT-mCherry intracerebroventricular injection. Body weight gain, adipose tissue weight, food intake, glucose metabolism, c-Fos, and neuropeptide expression were evaluated at 4 weeks post-transduction.

Results: Tanycytes sequester glucose-6-phosphate (G6P) into the ER through the G6Pase system and release glucose in hypoglycaemia via facilitative glucose transporters (GLUTs). Strikingly, *in vivo* tanycytic *G6pt* knockdown has a powerful peripheral anabolic effect observed through decreased body weight, white adipose tissue (WAT) tissue mass, and strong downregulation of lipogenesis genes. Selective deletion of *G6pt* in tanycytes also decreases food intake, c-Fos expression in the arcuate nucleus (ARC), and *Npy* mRNA expression in fasted mice.

Conclusions: The tanycyte-associated G6Pase system is a central mechanism involved in controlling metabolism and energy balance.

© 2024 The Authors. Published by Elsevier GmbH. This is an open access article under the CC BY-NC license (http://creativecommons.org/licenses/by-nc/4.0/).

Keywords Tanycytes; G6Pase system; Hypoglycaemia; Energy balance

1. INTRODUCTION

In 1975, Arion and colleagues discovered that hepatocytes release glucose into the bloodstream in response to hypoglycaemia using the glucose-6-phosphatase (G6Pase) system [1]. This system is in the endoplasmic reticulum (ER) and is composed of two functionally linked proteins, a G6P transporter subunit (G6PT) and a catalytic subunit called G6P phosphatase (G6Pase) [2,3]. The G6PT subunit promotes the storage of G6P inside the ER, while G6Pase, which has its catalytic domain in the reticular lumen, hydrolyses G6P to yield free glucose + phosphate [2,4–6]. The free glucose stored in the reticular lumen can be transported to the cytosol and from there to the extracellular space in hypoglycaemic conditions by a direct mechanism that has not yet been established [7], but eventually by glucose transporters (GLUTs) [2,3,8].

The G6Pase system has been extensively studied in organs that export glucose, such as the liver and, to a lesser extent, the kidney. However, in 2018, Müller and colleagues demonstrated that the G6Pase system is also expressed in astrocyte-type glial cells [7,9–11]. In this context, it was shown that human fetal astrocytes express the G6PT subunit and isoform 3 of G6Pase, also called G6PC3 [9]. Additionally, it was determined that astrocytes sequester glucose in the ER and that it is hydrolysed in the reticular lumen by the action of the G6PC3 catalytic subunit [9]. These surprising findings led to the proposal of a completely innovative concept for the ER of astrocytes. This proposal states that the ER can sequester glucose by using the G6Pase system and can also provide protected transport of this molecule from sites of glucose uptake to places where energy is needed. However, it is unknown whether other glial cells use this system as a mechanism of communication with nearby cells.

[1]Laboratory of Neurobiology and Stem Cells, NeuroCellT, Department of Cellular Biology, Faculty of Biological Sciences, University of Concepcion, Concepcion, Chile [2]Center for Advanced Microscopy CMA BIO BIO, University of Concepcion, Concepcion, Chile [3]Laboratory of Appetite Physiology (FIDELA), Faculty of Medicine and Sciences, University San Sebastián, Concepción Campus, Concepción, Chile

*Corresponding author. Departamento de Biología Celular, Facultad de Ciencias Biológicas, Universidad de Concepción, Concepción, Chile. Tel.: +56 41 220 3479. E-mail: frnualart@udec.cl (F. Nualart).

Abbreviations: G6PT, glucose-6-phosphate transporter; G6Pase, glucose-6-phosphatase; G6P, glucose-6P; ER, endoplasmic reticulum; GLUT1, glucose transporter 1; GLUT6, glucose transporter 6; GLUT2, glucose transporter 2; NPY, neuropeptide Y; POMC, proopiomelanocortine; CHA, chlorogenic acid; Thi, thielavin; 3V, third ventricle; CSF, cerebral spinal fluid; ARC, arcuate nucleus.

Received January 10, 2024 • Revision received April 9, 2024 • Accepted April 9, 2024 • Available online 17 April 2024

https://doi.org/10.1016/j.molmet.2024.101940

 © 2024 The Authors. Published by Elsevier GmbH. This is an open access article under the CC BY-NC license (http://creativecommons.org/licenses/by-nc/4.0/).

After 30 years from the discovery of Arion and colleagues, we show for the first time that the G6Pase system is also present in hypothalamic tanycytes. Tanycytes are glial cells that form the walls of the hypothalamic third ventricle (3 V) [12]. Their apical side is in direct contact with the cerebrospinal fluid (CSF), while their elongated processes are in close contact with neurons located in hypothalamic nuclei to regulate energy homeostasis [13,14]. Using 4-dimensional live-cell microscopy, we determined that tanycytes sequester G6P in the ER using the G6Pase system. Interestingly, we have detected that in hypoglycaemic conditions, tanycytes can release pulses of glucose from the ER using GLUTs. Surprisingly, *in vivo* knockdown of the G6Pase system generated through knockdown of *G6pt* induces a decrease in body weight and disturbs peripheral lipid homeostasis. Moreover, selective silencing of *G6pt* in tanycytes decreases food consumption, ARC c-Fos expression and downregulates *Npy* gene expression in response to food deprivation. In conclusion, the G6Pase system associated with tanycytes is a critical mechanism for regulating energy homeostasis and is, perhaps, a possible therapeutic target against obesity.

2. MATERIALS AND METHODS

2.1. Compounds

Thielavin A (Santa Cruz Biotech, #CAS 71950-66-8), Chlorogenic acid (Sigma—Aldrich, #C3878), BAY-876 (Cayman, #1799753-84-6), and Glutor (Sigma—Aldrich, #SML2765).

2.2. Mice

C57BL/6J mice were maintained at 23 °C and 40% humidity with a 12 h light/dark (07:00 a.m on-07:00 p.m off) cycle. For all physiological studies, 8-week-old male mice were used. Four to six mice were housed per cage and randomly chosen for each experiment. Animals were fed ad libitum with a standard rodent diet (LabDiet, Diet 5001), except under experimental conditions. For the food intake experiments, mice were individually housed 1 week before the experiment. All experiments were approved by the Animal Ethics Committee of the National Research and Development Agency (ANID, project protocol #3210076), and the animals were handled following the Guide for the Care and Use of Laboratory Animals (NRC 2011).

2.3. Primary culture of tanycytes

Postnatal stage 3 (P3) mice were used for primary cell cultures. The tanycytes were isolated from the ARC/ME region as previously described [15,16]. Subsequently, isolated ARC/MEs were dissociated in a 0.25% trypsin-0.2% EDTA (w/v) solution (Thermo Fisher, # 25200056) for 20 min at 37 °C. Cells were maintained at 37 °C and 5% v/v CO2 in a humidified incubator with MEM (GIBCO, #61100053) supplemented with 10% FBS (Mediatech, #MD.35-010-CV), 100 U/mL penicillin–streptomycin (GIBCO), and 2 mM L-glutamine (GIBCO). After 1h, the culture medium was changed to MEM supplemented with 10% FBS (Mediatech, #MD.35-010-CV), 100 U/mL penicillin–streptomycin (GIBCO), and 2 mM L-glutamine (GIBCO). The medium changes were performed every 2 days. All experiments were performed on Day 14 *in vitro.*

2.4. In vitro 2-NBDG analysis

For confocal analysis, 3,000 cells were seeded in glass bottom microplates (Greiner Bio-One, #655892). One day after seeding, cells were transduced with 50 particles of the CellLight™ ER-RFP construct, BacMam 2.0 (Thermo Fisher, #C10591), for 40 h. During this period, cells were incubated with MEM (GIBCO, #61100053) supplemented with 5% FBS (Mediatech, #MD.35-010-CV), 100 U/mL penicillin–streptomycin (GIBCO), and 2 mM L-glutamine (GIBCO). Forty hours post-transduction, cultures were incubated with Thielavin-A (20 μM), Chlorogenic acid (100 μM), or a combinatorial cocktail of Thielavin-A (20 μM) and Chlorogenic acid (100 μM) in MEM for 1 h before the experiment. Subsequently, the cultures were washed three times with DMEM without glucose and without serum but supplemented with 100 U/mL penicillin–streptomycin (GIBCO) and 2 mM L-glutamine (GIBCO). Cultures were then incubated with the fluorescent glucose probe, 2-NBDG (200 μM). Incubation was carried out for 30 min at 37 °C. Subsequently, the cultures were washed three times with DMEM without glucose, and live-cell photographs were obtained using an SP8 confocal-spectral microscope and postprocessed using the Lightning SuperResolution module. Finally, the images were analysed using IMARIS software (Oxford instruments). Colocalization images were obtained between the ER-RFP label and the 2-NBDG probe. Additionally, the fluorescence intensity of the green channel (2-NBDG) over the red channel (ER-RFP) was calculated for each condition ($n = 7-13$ cells, three independent cultures).

2.5. Real-time 2-NBDG-ER retention

For the experiments, 3,000 tanycytes were seeded in 96-well plates (Merck, Corning # CLS3370). Subsequently, cultures were transduced with CellLight™ ER-RFP construction as previously described (*In vitro* 2-NBDG analysis section). Subsequently, cultures were incubated with Bay-876 (10 μM) or Glutor (5 μM) for 1 h. Next, cultures were washed three times with DMEM without glucose and serum but supplemented with 100 U/mL penicillin–streptomycin (GIBCO) and 2 mM L-glutamine (GIBCO). Cells were next incubated with 200 μM of the 2-NBDG probe for 30 min at 37 °C followed by three washes to remove excess 2-NBDG. The plate was immediately subjected to analysis by the real-time monitoring instrument IncuCyte S3 (Sartorius). Experiments were performed in three to five independent cultures, and four photos were taken per condition.

2.6. Immunocytochemistry

For immunolocalization analyses, cells were plated on glass coverslips at a density of 8,000 cells/well (2.0 cm^2). Subsequently, the cells were fixed with 4% paraformaldehyde (PFA) for 30 min at room temperature. Next, three washes of 10 min each with tris-phosphate buffer were performed. Finally, the cells were incubated with the following primary antibodies: mouse anti-G6PT (1:200), rabbit anti-G6PT (1:200), chicken anti-vimentin (1:500), rabbit anti-connexin-43 (1:300), DARPP-32 (1: 100), rabbit anti-GFAP (1:200), rabbit anti-GLUT1 (1:500), rabbit anti-GLUT2 (1:200), mouse anti-GLUT6 (1:200), and rabbit anti-G6pc3 (1:200) overnight at room temperature. Subsequently, three washes were carried out with tris-phosphate buffer, and the coverslips were incubated for 2 h with secondary antibodies (The Jackson Laboratory). Hoechst 33342 (1:1000) was used for nuclear staining. The images were obtained with an SP8 spectral confocal microscope (Leica) and were processed with the Lightning Super-Resolution module. All the information about the primary antibodies used in this work can be found in Table 1.

2.7. Adeno-associated virus (AAV) delivery

For these studies, 8-week-old male mice were used. Mice were anesthetized with isoflurane and placed in the stereotaxic frame (RWD, # 68037). Next, using a microinjection syringe pump (WPI, # UMP3T-1), 2 μL of the AAV control AAV_1-mCherry-U6>Scramble (Vector Builder, ID: VB010000-0024wah, title, $>10^{12}$G) or *G6pt* knockdown AAV_1-mCherry-U6>m*Slc37a4* (Vector Builder, ID: VB210324-

 © 2024 The Authors. Published by Elsevier GmbH. This is an open access article under the CC BY-NC license (http://creativecommons.org/licenses/by-nc/4.0/).

Table 1 — List of antibodies used for immunocytochemistry and immunohistochemistry analysis.

Antigen	Immunogen	Manufacturer	Cat number	Species
Glucose-6-phosphate transporter (G6PT)	Amino acids 28—76 of G6PT of human origin	Santa Cruz biotech	sc-293321	Mouse
Glucose-6-phosphate transporter (G6PT)	Recombinant protein corresponding to amino acids: LDKDDLGFITSSQSAAYAISKFVSGVLSDQMS	Novus biologicals	NBP2-31972	Rabbit
Vimentin	Recombinant vimentin	Sigma—Aldrich	AB5733	Chicken
Connexin 43	Synthetic peptide corresponding to the C-terminal segment of the cytoplasmic domain (amino acids with N-terminally added lysine) of human/rat connexin-43	Sigma—Aldrich	C6219	Rabbit
DARPP-32	Epitope mapping between amino acids 2—34 at the N-terminus of DARPP-32 of human origin	Santa Cruz biotech	sc-271111	Mouse
Glial Fibrillary Acidic Protein (GFAP)	GFAP isolated from cow spinal cord	Dako	Z0334	Rabbit
Glucose transporter 1 (GLUT1)	Synthetic peptide corresponding amino acids with the C-terminus of human GLUT-1 coupled to KLH (C-ELFHPLGADSQV)	Sigma—Aldrich	07—1401	Rabbit
Glucose transporter 2 (GLUT2)	16-aa peptide from Rat Glut-2; Designation (GT21-P, control peptide/blocking peptide) conjugated to KLH; Epitope locatioñ C-terminal, Cytoplasmic domain	Alpha diagnostic	GT21-A	Rabbit
Glucose transporter 6 (GLUT6)	Synthetic peptide	Abcam	ab118025	Mouse
Glucose 6 phosphatase 3 (G6pc3)	Synthetic peptide directed towards the N-terminal region of human G6PC3	ThermoFisher	PA5-70653	Rabbit
c-Fos	synthetic peptide corresponding to residues near the amino terminus of human c-Fos protein	Cell Signaling Technology	2250	Rabbit

1260vvu, title, $>10^{12}$G) were infused into the 3 V (anteroposterior, −1.8 mm; midline, 0 mm; dorsoventral, −5.5 mm). It is important to mention that serotype 1 AAVs do not traverse the parenchyma and, moreover, can specifically infect tanycytes [17]. All experiments were performed at 4 weeks post-transduction, and analgesia was applied following the previously described recommendations [18].

2.8. In vivo G6PT silencing analysis

For G6PT protein levels, *G6pt*^{TanScramble} (n = 3) and *G6pt*^{TanKD} (n = 3) mice were sacrificed, and the hypothalamic region of the brain was harvested and added to RIPA buffer (Thermo Fisher Scientific #89901) supplemented with Protease/Phosphatase Inhibitor Cocktail (Cell Signaling #5872). Proteins were then extracted by sonication and quantified as described above (see *in vitro* immunoblot section). Fifty micrograms of total protein extract were separated using TGX FastCast Acrylamide 10% gels (Bio-Rad #1610173). After the proteins were transferred to PVDF membranes (0.45-μm pore; Immobilon-P #IPVH00010, Merck Millipore), the membrane was incubated at 4 °C overnight with the rabbit anti-G6PT primary antibody (1:500). Next, the membrane was washed and incubated with the rabbit-HRP secondary antibody for 2 h. HRP-conjugated anti-actin antibody (1:20000) was used as a loading control. For mRNA *G6pt* expression, *G6pt*^{TanScramble} (n = 6) and *G6pt*^{TanKD} (n = 6) mice were sacrificed, and the hypothalamic area was collected. Total RNA extraction was performed using TRIzol reagent (Ambion). Quantitative real-time PCR was carried out in a Mastercycler Realplex2 (Eppendorf). The primer gene information can be found in Supplementary Table 1.

2.9. Immunohistochemistry

Untreated 4-week-old transduced C57BL/6J mice were anesthetized with isoflurane and sacrificed by cervical dislocation. Subsequently, mice were transcardially cannulated, washed with 1X PBS buffer, and fixed with 4% PFA. Next, the harvested brains were embedded in a 30% sucrose solution for 72 h and frozen in a cryopreservative solution (NEG-50 Frozen Section Medium). Frontal hypothalamic sections of 20 μm each were obtained using a cryostat (Thermo Fisher, #HM525) and mounted on polylysine-treated slides. Next, three washes of 10 min each were performed in 1X tris-phosphate buffer followed by incubation in the following primary antibodies: rabbit anti-G6PT (1:50), mouse anti-G6PT (1:50), chicken anti-vimentin (1:400), rabbit anti-GFAP (1:200), rabbit anti-GLUT1 (1:500), rabbit anti-GLUT2 (1:200), mouse anti-GLUT6 (1:200), and chicken anti-vimentin (1:400) overnight at room temperature. Subsequently, sections were washed three times for 10 min with tris-phosphate buffer and incubated with the secondary antibody (The Jackson Laboratory). Hoechst 33342 (1:1000) was used for nuclear staining. The images were obtained with an SP8 spectral confocal microscope (Leica) and were postprocessed with the Lightning SuperResolution module. For fasted-refed G6pc3 expression, mice were basal fed (n = 6) or fasted (n = 7) for 24 h prior to the experiment. The fluorescence intensity fold change of G6pc3 was analysed using ImageJ software. All information about the primary antibodies used in this work can be found in Table 1.

2.10. Mouse physiology

G6pt^{TanScramble} and *G6pt*^{TanKD} 8-week-old male mice were injected and weighed weekly (05:00 p.m.) for 4 weeks post-transduction using an analytical balance (n = 10—12 mice per condition). The delta of body weight (BW) after injection was calculated by the difference in BW (g) between w0-w1, w1-w2, w2-w3 and w3-w4 (n = 8—12 mice per treatment). BW gain at 2 weeks was represented as BW gain (g) between the week (w0) of surgery and 2 weeks post-transduction (n = 10—12 mice per treatment). BW gain at 4 weeks was represented as BW gain (g) between the week (w0) of surgery and 4 weeks post-transduction (n = 10—12 mice per treatment). For food intake experiments, *G6pt*^{TanScramble} and *G6pt*^{TanKD} mice were individually housed 1 week before the experiment. For basal food intake in the dark and light cycles, food intake was measured at 12 h and 24 h after feeding (n = 6—9 mice per condition). For short-term feeding, food intake was measured at 1 and 2 h after feeding (n = 6—9 mice per condition). For trials of food intake in response to fasting, *G6pt*^{TanScramble} and *G6pt*^{TanKD} mice were fasted for 24 h before starting the experiment (n = 7—8 mice per condition). Food intake in response to fasting during the night or day was measured at 12 h and 24 h after feeding (n = 7—8 mice per condition). Short-term feeding in response to fasting was measured at 1 and 2 h after feeding (n = 7—8 mice per condition). All food intake measurements were performed by the same researcher.

2.11. Glucose metabolism

Blood glucose levels were analysed in *G6pt*^{TanScramble} (n = 4) and *G6pt*^{TanKD} (n = 4) mice at the end of a 24 h fasting or a 24 h fed period. For glucose tolerance tests (GTTs), both *G6pt*^{TanScramble} and *G6pt*^{TanKD} mice were intraperitoneally injected with a 30% glucose solution (1 μL/

 © 2024 The Authors. Published by Elsevier GmbH. This is an open access article under the CC BY-NC license (http://creativecommons.org/licenses/by-nc/4.0/).

g of body weight) after 16 h of fasting. Blood glucose levels were measured at 0-, 30-, 60-, and 120-minutes post-injection. Blood samples were obtained from the tail, and glucose levels were analysed using a glucose meter (Accu-chek Performa). All analyses were performed at 4 weeks post-transduction.

2.12. Insulinemia and glucagonemia

G6pt^{TanScramble} (n = 5–7) and *G6pt*^{TanKD} (n = 4–5) mice were fed ad libitum. Subsequently, a blood sample was obtained by facial vein puncture. Insulin and glucagon levels were analysed in serum samples using the MILLIPLEX Mouse Metabolic Hormone Expanded Panel (Merck, #MMHE-44K). Hormone levels were calculated using the Luminex MAGPIX system (Luminex). All analyses were performed at 4 weeks post-transduction.

2.13. Neuropeptide gene expression

G6pt^{TanScramble} (n = 3–5) and *G6pt*^{TanKD} (n = 4–5) mice were ad libitum fed (10:00 a.m.-10:00 a.m.) or fasted for 24 h (10:00 a.m.-10:00 a.m.). In this context, the following experimental groups were created: Group 1, *Ad-libitum* fed *G6pt*^{TanScramble} mice; Group 2, *Ad-libitum*-fed *G6pt*^{TanKD} mice; Group 3, 24 h fasted *G6pt*^{TanScramble} mice; and Group 4, 24 h fasted *G6pt*^{TanKD} mice. Next, mice were anesthetized and sacrificed by cervical dislocation. Subsequently, the hypothalamic region was dissected at the level of the optic chiasm and stored in TRIzol reagent (Ambion) at −80 °C. cDNA was obtained using the High-Capacity cDNA Reverse Transcription Kit (Applied Biosystems), and quantitative real-time PCR was performed to analyse *Npy* and *Pomc expression* levels. The primers used to generate the qRT–PCR amplification products are shown in Supplementary Table 1. *Gapdh* was used as a housekeeping gene.

2.14. Statistical analysis

All values are expressed as the mean ± standard error of the mean (SEM). For each of the experiments, the animals were chosen randomly using the simple random sample method. No animal was excluded from either the experiments or the statistical analysis. No blinding and no sample calculation were performed in the experiments. *t* tests were used to compare two groups, and ANOVA (followed by Bonferroni's *post hoc test)* was used for multiple comparisons using GraphPad Prism 5.0 Software (GraphPad Software). The number of animals for each experiment, the statistical tests applied, the confidence intervals and the statistical values are presented in Table 2.
A full and detailed description of all our methods is available in the Supplemental Material.

3. RESULTS

3.1. Hypothalamic tanycytes express components of the G6Pase system

First, we evaluated the presence of the G6Pase system in tanycytes *in vitro*. As shown in Figure 1A, primary tanycyte cultures express classic markers of tanycytes, such as the intermediate filament marker vimentin, connexin 43, and DARPP-32 [19]. It is important to mention that the cultures show low immunoreactivity for the intermediate filament, GFAP, indicating that the generated culture is enriched in tanycytes and not other glial cells, such as astrocytes (Figure 1A). Interestingly, we determined that tanycytes express *G6pt* mRNA *in vitro* but at lower levels of expression compared to the liver (Figure 1B). Additionally, also express the protein of G6PT subunit (Supplementary Figure 1A-B). *In vitro* tanycytes, expressed the G6PT subunit in colocalization with the tanycyte marker, vimentin (Figure 1C). To test the subcellular localization of G6PT, we transduced cultures with the ER-RFP baculovirus, a construct that expresses RFP in fusion to the ER signal sequence of calreticulin and KDEL. As shown in Figure 1D, baculovirus transduced tanycytes *in vitro*. Intracellular RFP fluorescence was detected exclusively in structures similar to the ER (Figure 1D, arrow). Quantification of the transduction percentage using the IncuCyte live-cell monitoring system showed an efficiency close to 50% transduction at 40 h post-transduction (Figure 1E). Therefore, subcellular localization studies were conducted starting from 40 h post-transduction. As observed in Figure 1F, G6PT was exclusively localized in the ER of tanycytes (Figure 1F, arrow). To determine the level of colocalization between RFP and G6PT, we calculated Pearson's correlation index using an ROI restricted to the reticular area. The Pearson's index was 0.599, indicating a high degree of colocalization between the ER marker and G6PT (Figure 1G).
Preliminary reports have described the existence of three genes that encode three subunits of G6P phosphatase known as *G6pc1*, *G6pc2*, and *G6pc3* [20]. We observed that *in vitro* tanycytes express mainly the G6pc3 catalytic subunit (also known as isoform β), similar to what has been previously reported in mouse astrocytes and human foetal astrocytes (Figure 1H–I, arrow) [9,10]. It is important to mention that the G6pc3 catalytic subunit, similar to G6PT, is located in the ER of tanycytes (Figure 1J, arrow). The Pearson's correlation index between RFP and G6Ppc3 was 0.485, indicating a high degree of colocalization between the ER marker and G6pc3 (Figure 1K).
In the next stage, we analysed whether components of the G6Pase system are expressed in tanycytes *in vivo*. Thus, we analysed the expression and localization of G6PT and G6pc3 in the hypothalamic tissue of fed adult mice. Interestingly, low- and high-magnification images show intense immunoreactivity for G6PT at the apical area of the cells (Figure 1L, arrow) and in the processes of vimentin-positive β1-2 tanycytes that contact the ARC and form the median eminence (ME), respectively (Figure 1L, asterisks) (Supplemental Figure 2C-E, arrowhead). It is important to mention that immunoreactivity for G6PT was not detected in either ependymocytes or in the GFAP-positive α-tanycyte population (Supplemental Figure 2A-B, arrowhead). Additionally, G6PT expression was not detected in other hypothalamic cell types, such as GFAP-positive astrocytes or blood vessels (Supplemental Figure 3A-B, arrows). A similar scenario was observed when analysing the expression and distribution of G6pc3. Interestingly, low- and high-magnification images show intense immunoreactivity for G6pc3 at the apical area (Figure 1M, arrow) and in the processes of vimentin-positive β1-2 tanycytes (Figure 1M, asterisks).
Consistent with this notion, the results show that *in vitro* and *in vivo* tanycytes possess the G6Pase system. Therefore, they are molecularly equipped to sequester G6P from the cytosol to the ER and hydrolyse G6P in the ER lumen.

3.2. Tanycytes sequester glucose into the ER using the G6Pase system

Previous studies conducted in microsomes have shown that the G6Pase system promotes the uptake of G6P from the cytosol into the reticular lumen [2,21,22]. To determine if this also occurs in tanycytes, we analysed the uptake of reticular G6P using the fluorescent glucose analogue, 2-NBDG (Figure 2A). Importantly, 2-NBDG is intracellularly phosphorylated, favouring its retention inside the cell [23,24], and is used to evaluate reticular G6P uptake [25]. Using tanycytes transduced with the ER-RFP baculovirus and 4D live-cell microscopy, 2-NBDG probe sequestration was observed in the ER (Figure 2B, arrow). To determine the level of colocalization between RFP and the 2-NBDG probe, we calculated Pearson's correlation index using an ROI

 © 2024 The Authors. Published by Elsevier GmbH. This is an open access article under the CC BY-NC license (http://creativecommons.org/licenses/by-nc/4.0/).

Table 2 — Results of statistical analysis unpaired t-test, one-way ANOVA and two-way ANOVA.

Figure	Stadistic test	n	Data reported	p-value	F(DFn. DFd)	t. df
Figure 1B	Unpaired t-test	n = 4–5	Mean ± SEM	P < 0.0001		t = 9.368 df = 6
Figure 1H	One-way ANOVA	n = 9–7	Mean ± SEM	P < 0.0001	F (2,21) = 44.68	
Figure 2H	One-way ANOVA	n = 7–13	Mean ± SEM	P < 0.0001	F (3,30) = 20.50	
Figure 3A (glucose response)	Unpaired t-test	n = 12	Mean ± SEM	P = 0.0104		t = 2.492 df = 22
Figure 3A (nutritional response)	Unpaired t-test	n = 6–7	Mean ± SEM	P < 0.0001		t = 6.202 df = 11
Figure 3C	Unpaired t-test	n = 3–8	Mean ± SEM	P < 0.0001		t = 13.25 df = 9
Figure 3E	Unpaired t-test	n = 3	Mean ± SEM	P = 0.0140		t = 3.372 df = 4
Figure 3F	Unpaired t-test	n = 5–6	Mean ± SEM	P = 0.2313		t = 0.7672 df = 9
Figure 3G	Unpaired t-test	n = 7–9	Mean ± SEM	P = 0.0270		t = 2.104 df = 14
Figure 3I	One-way ANOVA	n = 3–5	Mean ± SEM	P = 0.0267	F (2,10) = 5.317	
Figure 4C	Unpaired t-test	n = 6	Mean ± SEM	P = 0.0217		t = 2.311 df = 10
Figure 4E	Unpaired t-test	n = 3–4	Mean ± SEM	P < 0.0001		t = 6.077 df = 5
Figure 4F	Two-way ANOVA	n = 8–12	Mean ± SEM	Interaction: P = 0.7698 Row factor: P = 0.0135 Column factor: P < 0.0001	Interaction: F (4,93) = 0.4533 Row factor: F (4,93) = 3.332 Column factor: F (1,93) = 17.76	
Figure 4G	Unpaired t-test	n = 13	Mean ± SEM	P = 0.0007		t = 3.627 df = 24
Figure 4H	Unpaired t-test	n = 10	Mean ± SEM	P = 0.0002		t = 4.368 df = 18
Figure 4I	Unpaired t-test	n = 13–14	Mean ± SEM	P = 0.1862		t = 0.9084 df = 25
Figure 4J	Unpaired t-test	n = 4–5	Mean ± SEM	P = 0.6259		t = 0.5136 df = 6
Figure 4K	Unpaired t-test	n = 7–10	Mean ± SEM	P = 0.0009		t = 3.783 df = 15
Figure 4L	Unpaired t-test	n = 6–11	Mean ± SEM	P = 0.0293		t = 2.046 df = 15
Figure 4M	One-way ANOVA	n = 6–10	Mean ± SEM	P < 0,0001	F(3, 28) = 95.03	
Figure 4N	Unpaired t-test	n = 6	Mean ± SEM	P = 0.0019		t = 3.756 df = 10
Figure 4O	Unpaired t-test	n = 6	Mean ± SEM	P < 0.0001		t = 5.756 df = 10
Figure 4P	Two-way ANOVA	n = 4–6	Mean ± SEM	Interaction: P = 0.4466 Row factor: P = 0.0007 Column factor: P = 0.6713	Interaction: F (3,30) = 0.9127 Row factor: F (1,30) = 14.23 Column factor: F (3,30) = 0.5207	
Figure 4Q	Two-way ANOVA	n = 4–7	Mean ± SEM	Interaction: P = 0.5704 Row factor: P = 0.0010 Column factor: P = 0.5489	Interaction: F (2,28) = 0.5729 Row factor: F (1,28) = 13.38 Column factor: F (2,28) = 0.6128	
Figure 5B	Unpaired t-test	n = 6–9	Mean ± SEM	P = 0.0813		t = 1.480 df = 13
Figure 5C	One-way ANOVA	n = 6–9	Mean ± SEM	P = 0.0191	F (3, 26) = 25.98	
Figure 5D	One-way ANOVA	n = 6–9	Mean ± SEM	P = 0.0321	F (3, 26) = 3.417	
Figure 5F	One-way ANOVA	n = 7–16	Mean ± SEM	P = 0.3236	F (3, 39) = 1.197	
Figure 5G	Unpaired t-test	n = 7–8	Mean ± SEM	P = 0.0222		t = 2,226 df = 13
Figure 5H	One-way ANOVA	n = 7–8	Mean ± SEM	P = 0.0731	F (3, 26) = 26.71	
Figure 5I	One-way ANOVA	n = 7–8	Mean ± SEM	P = 0.0320	F (3, 25) = 3.442	
Figure 5J (*G6pt*^{Tanscramble})	Unpaired t-test	n = 6	Mean ± SEM	P = 0.0216		t = 2.313 df = 10
Figure 5J (*G6pt*^{TankD})	Unpaired t-test	n = 8–9	Mean ± SEM	P = 0.3406		t = 0,4188 df = 15
Figure 5K (*G6pt*^{Tanscramble})	Unpaired t-test	n = 6–7	Mean ± SEM	P = 0.0107		t = 2.682 df = 11
Figure 5K (*G6pt*^{TankD})	Unpaired t-test	n = 7–9	Mean ± SEM	P = 0.1670		t = 1.001 df = 14
Figure 5L	One-way ANOVA	n = 5–12	Mean ± SEM	P = 0.3915	F (7, 51) = 5.940	
Figure 6A	Unpaired t-test	n = 4	Mean ± SEM	P = 0.4825		t = 0.04584 df = 6
Figure 6B	Unpaired t-test	n = 4	Mean ± SEM	P = 0.4474		t = 0.1381 df = 6
Figure 6C	Two-way ANOVA	n = 4	Mean ± SEM	Interaction: P = 0.8985 Row factor: P < 0.0001 Column factor: P = 0.6048	Interaction: F (4, 29) = 0.2643 Row factor: F (4, 29) = 11.63 Column factor: F (1, 29) = 0.2737	
Figure 6C (AUG)	Unpaired t-test	n = 4	Mean ± SEM	P = 0.4041		t = 0.2536 df = 6
Figure 6D	Unpaired t-test	n = 5	Mean ± SEM	P = 0.051		t = 1.847 df = 8
Figure 6E	Unpaired t-test	n = 4–7	Mean ± SEM	P = 0.3720		t = 0.3369 df = 9
Figure 7A	Unpaired t-test	n = 5	Mean ± SEM	P = 0.1596		t = 1.062 df = 8
Figure 7B	Unpaired t-test	n = 4–5	Mean ± SEM	P = 0.0375		t = 2.090 df = 7
Figure 7C	Two-way ANOVA	n = 4–5	Mean ± SEM	Interaction: P = 0.0895 Row factor: P = 0.0006 Column factor: P = 0.0028	Interaction: F (1,13) = 3.368 Row factor: F (1,13) = 20.24 Column factor: F (1,13) = 13.55	
Figure 7D	Two-way ANOVA	n = 4–5	Mean ± SEM	Interaction: P = 0.9819 Row factor: P = 0.9159 Column factor: P = 0.0013	Interaction: F (1,15) = 0.0005340 Row factor: F (1,15) = 0.01154 Column factor: F (1,15) = 15.41	

n, number of cultures or mice used in each experiment; SEM, standard error of the mean; F, F statistic; DFn, numerator degrees of freedom; DFd, denominator degrees of freedom; t, unpaired t-test statistic; df, degrees of freedom.

restricted to the reticular area. The Pearson's index was 0.5346, indicating a high degree of colocalization between the ER marker and the 2-NBDG probe (Figure 2C). To analyse whether 2-NBDG-ER uptake is dependent on the G6Pase system, we used two pharmacological inhibitors: the competitive inhibitor of G6PT, Chlorogenic acid (CHA, 100 μM), and the inhibitor of G6Pase, Thielavin A (Thi, 20 μM) (Figure 2D) [26–29]. It is important to mention that the concentrations of CHA and Thi used for these experiments do not generate lethal cytotoxic effects in the cultures (Figure 2E). Therefore, the effects observed in the incorporation of 2-NBDG into the ER can be attributed to the inhibition of the G6Pase system rather than the loss of cellular membrane integrity. Interestingly, we found that treatment with CHA

 © 2024 The Authors. Published by Elsevier GmbH. This is an open access article under the CC BY-NC license (http://creativecommons.org/licenses/by-nc/4.0/).

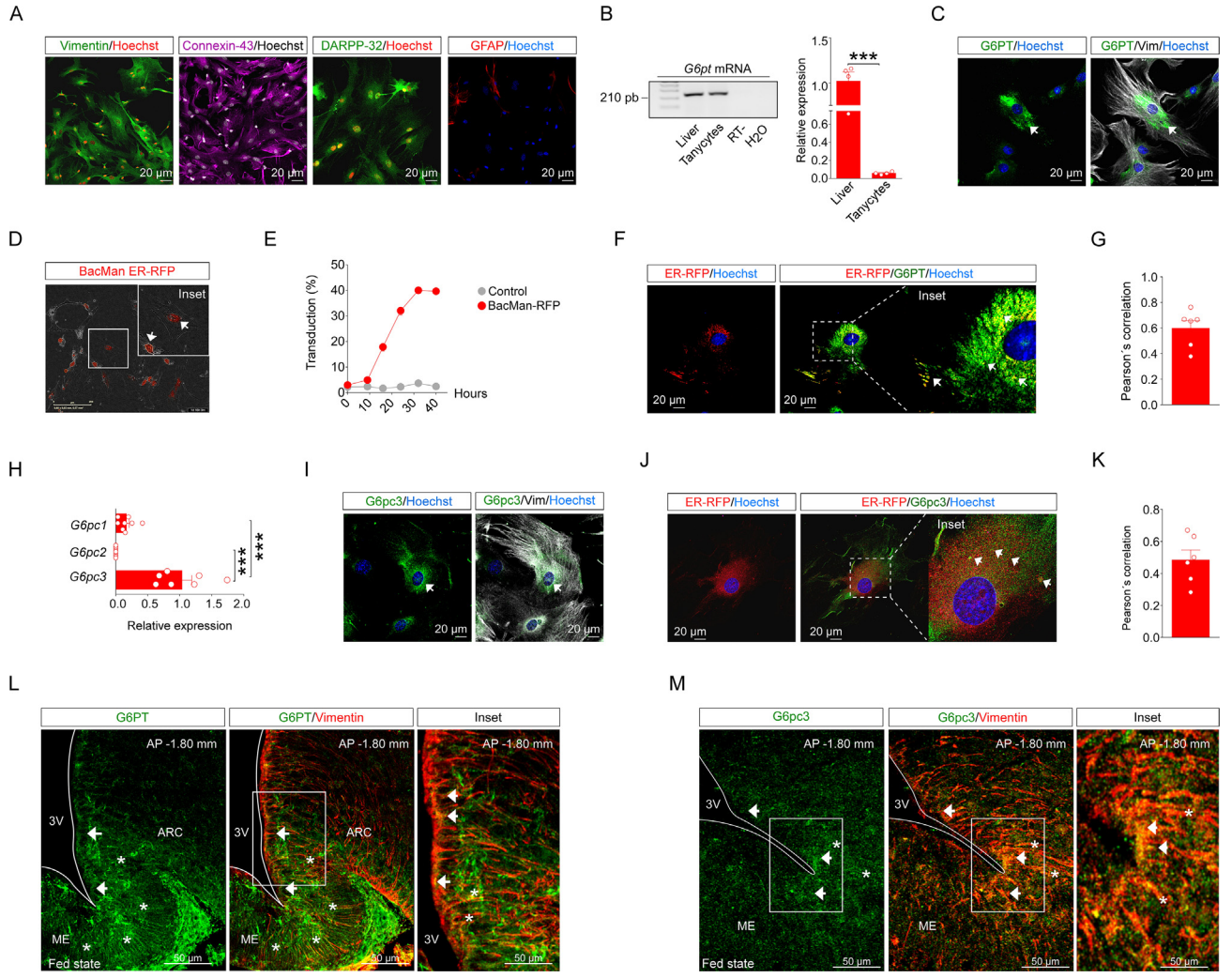

Figure 1: ***In vitro* and *in vivo* tanycytes express the G6Pase system. A**. Immunolocalization of vimentin (green), connexin-43 (magenta), DARPP-32 (green), and GFAP (red) in tanycytes *in vitro*. **B.** *G6pt* mRNA levels expression in tanycytes and mouse liver (n = 4–5). **C.** Immunolocalization of G6PT (green) and vimentin (white) in tanycytes *in vitro*. **D.** Culture of tanycytes transduced with the ER-RFP baculovirus. **E.** Percent transduction over time using the IncuCyte S3 real-time monitoring system (n = 5–9 wells). **F.** G6PT immunolocalization in tanycytes transduced with the ER-RFP baculovirus. **G.** Pearson's coefficient of the images obtained in F (n = 6 cells, three independent cultures). **H.** *G6pc1*, *G6pc2,* and *G6pc3* mRNA expression in tanycytes *in vitro* by qPCR (n = 7–9 independent cultures). **I.** Immunolocalization of G6pc3 (green) and vimentin (white) in tanycytes *in vitro*. **J.** G6pc3 immunolocalization in tanycytes transduced with the baculovirus, BacMan ER-RFP. **K.** Pearson's coefficient of the images obtained in J (n = 6 cells, three independent cultures). **L-M.** Immunolocalization of G6PT (green) and G6pc3 (green) in hypothalamic vimentin-positive (red) tanycytes of fed adult mice. Hoechst was used as a nuclear marker. *Gapdh* was used as a housekeeping gene for qPCR analyses. Data are represented as the mean ± SEM. Comparisons between more than two groups were made using one-way ANOVA. ***P < 0.001.

and Thi and cotreatment with CHA + Thi resulted in a decrease in the uptake of 2-NBDG at the ER level (Figure 2F, arrows). These findings were confirmed by generating a colocalization image using IMARIS software. In the control condition, a high degree of colocalization (yellow labelling) was detected between the ER marker (red labelling) and 2-NBDG probe (green labelling). However, the colocalization decreased when the cultures were incubated with CHA, Thi, or CHA + Thi (Figure 2G, arrow). Additionally, quantification of the fluorescence intensity (FI) of the 2-NBDG probe (green) over the ER marker (red) showed that cultures treated with CHA, Thi, and CHA + Thi exhibited a significant decrease in FI compared to that in cultures treated with the control condition (2-NBDG incubation without drug treatment) (Figure 2H). Therefore, the data strongly suggest that G6P uptake and storage in the tanycyte ER is mediated by the G6Pase system.

3.3. Glucose release from tanycytes during hypoglycaemia is modulated by the G6Pase system

In hypoglycaemic conditions, the G6Pase system promotes the release of glucose from the ER into the bloodstream to restore euglycemia [3]. Interestingly, we determined by immunodetection that hypoglycaemic conditions (1 mM glucose) upregulate the expression of the G6pc3 subunit both *in vitro* and *in vivo*, strongly suggesting that the G6pc3 subunit may promote G6P hydrolysis and the release of glucose pulses from tanycytes into the extracellular medium (Figure 3A, arrow), as previously reported in rat microsomes [1,30–32]. To test this hypothesis, we measured glucose release in glucose-restricted tanycyte cultures in the absence or presence of Thi (20 µM) (Figure 3B). Surprisingly, we determined that tanycytes release glucose in response to extracellular glucose restriction *in vitro*, and this metabolic reaction is dependent on the activity of G6pc3 (Figure 3C). Therefore, these

 © 2024 The Authors. Published by Elsevier GmbH. This is an open access article under the CC BY-NC license (http://creativecommons.org/licenses/by-nc/4.0/).

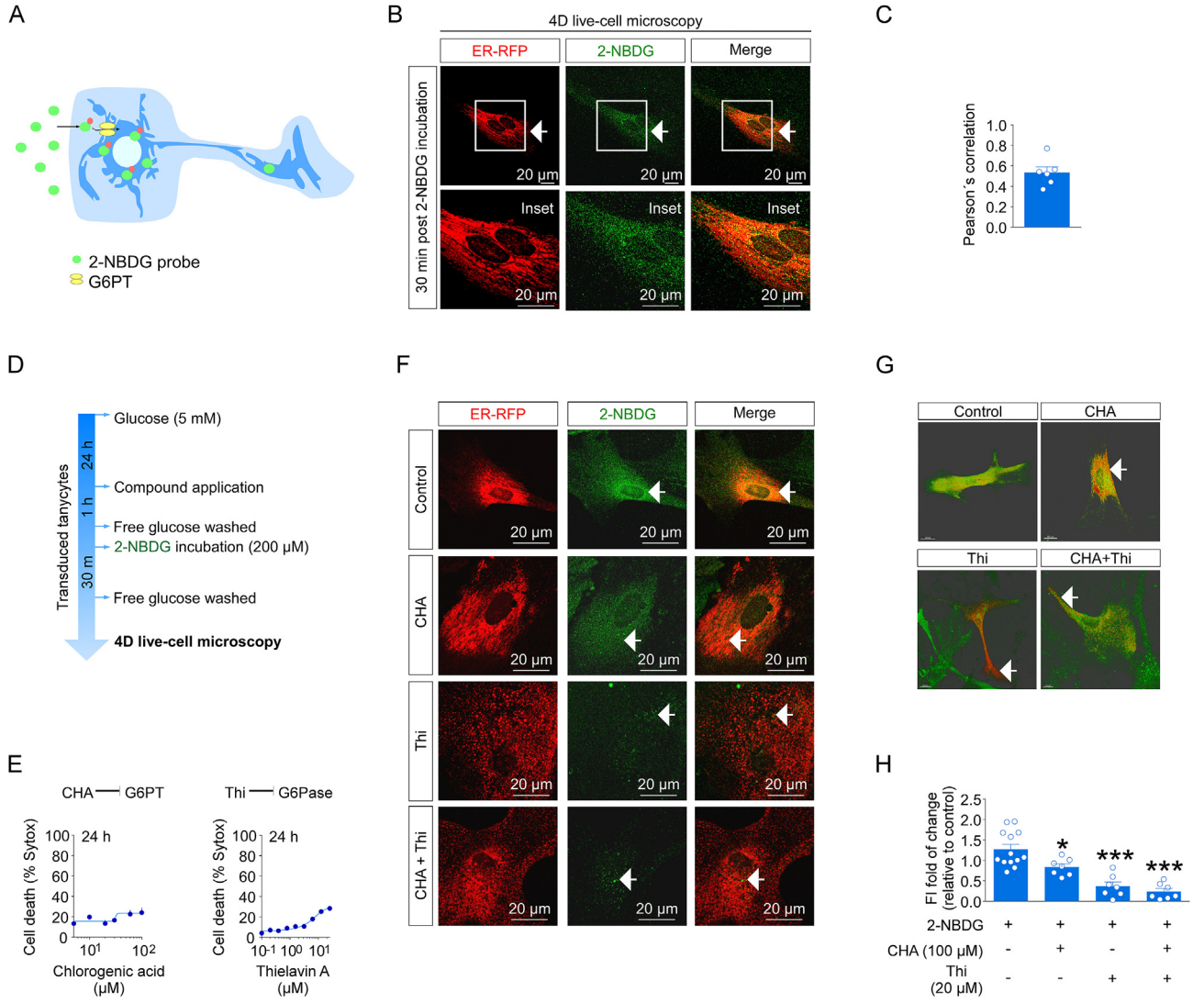

Figure 2: Tanycytes sequester G6P into ER-subcellular structures. A. Experimental protocol for live-cell microscopy studies using Lightning SuperResolution microscopy. **B.** Low- and high-magnification images of the colocalization of the 2-NBDG probe with the ER marker, ER-RFP. **C.** Pearson's coefficient of the images obtained in B ($n = 6$ cells, three independent cultures). **D.** Experimental protocol to evaluate uptake of the 2-NBDG probe in tanycytes incubated with CHA (100 µM), Thi (20 µM), or CHA + Thi. **E.** Lethality analysis using CHA and Thi. Percent cell death was calculated using the IncuCyte S3 system ($n = 3–4$ wells per condition). **F.** 2-NBDG uptake analysis in tanycytes transduced with ER-RFP baculovirus by live-cell microscopy. Tanycytes were incubated with CHA (100 µM) or Thi (20 µM) or coincubated with CHA + Thi. **G.** Colocalization images. The colocalization of the 2-NBDG probe and ER-RFP was evaluated in tanycytes treated with CHA (100 µM) or Thi (20 µM) or cotreated with CHA + Thi. Reconstructions were performed using IMARIS software. **H.** Fold change in fluorescence intensity (FI) of the reconstructions obtained in G ($n = 7–13$ cells, three independent cultures). Data are represented as the mean ± SEM. Comparisons between variables were made using one-way ANOVA. *$P < 0.05$, ***$P < 0.001$.

results suggest that tanycytes release glucose during hypoglycaemia from the ER-subcellular structures.

Currently, there are several hypotheses regarding how hydrolysed glucose is released from the ER into the extracellular medium during hypoglycaemia. One of them suggests that glucose can be released by GLUTs [8,33,34]. Preliminary studies have shown that *in vivo,* tanycytes express several GLUTs, such as GLUT1, GLUT2, and GLUT6 [12,35–37]. In line with these findings, we analysed the expression and distribution of these GLUTs in coronal sections of mice. As observed in Supplementary Figure 4A, GLUT1 was predominantly localized in vimentin-positive tanycyte processes, while GLUT2 and GLUT6 were primarily distributed in the apical region of these cells (Supplementary Figure 4B-C, arrow). Therefore, these findings suggest that these GLUTs may facilitate the export of glucose from the ER to the extracellular environment. To test this hypothesis, we identified the GLUTs that are expressed in ER of tanycytes. As shown in Figure 3D, *in vitro* tanycytes expressed GLUT1, GLUT2, and GLUT6 at the reticular level (Figure 3D, arrow). Using a colocation image obtained using IMARIS software, we were able to confirm our findings. The yellow colour in the images indicates that GLUT1, GLUT2, and GLUT6 are colocalized with RFP (Supplementary Figure 5A). Quantification of the % of volume GLUTs above threshold colocalized suggests that approximately 20% of the total volume occupied by GLUT1, GLUT2, and GLUT6 in the cell is located in the ER (Supplementary Figure 5B). To determine whether the global expression levels of GLUT1, GLUT2, and GLUT6 are modified in response to hypoglycaemia, we incubated the primary cultures with 5 mM (control condition) and 1 mM (hypoglycaemia condition) glucose. After 24 h of incubation, we evaluated

 © 2024 The Authors. Published by Elsevier GmbH. This is an open access article under the CC BY-NC license (http://creativecommons.org/licenses/by-nc/4.0/).

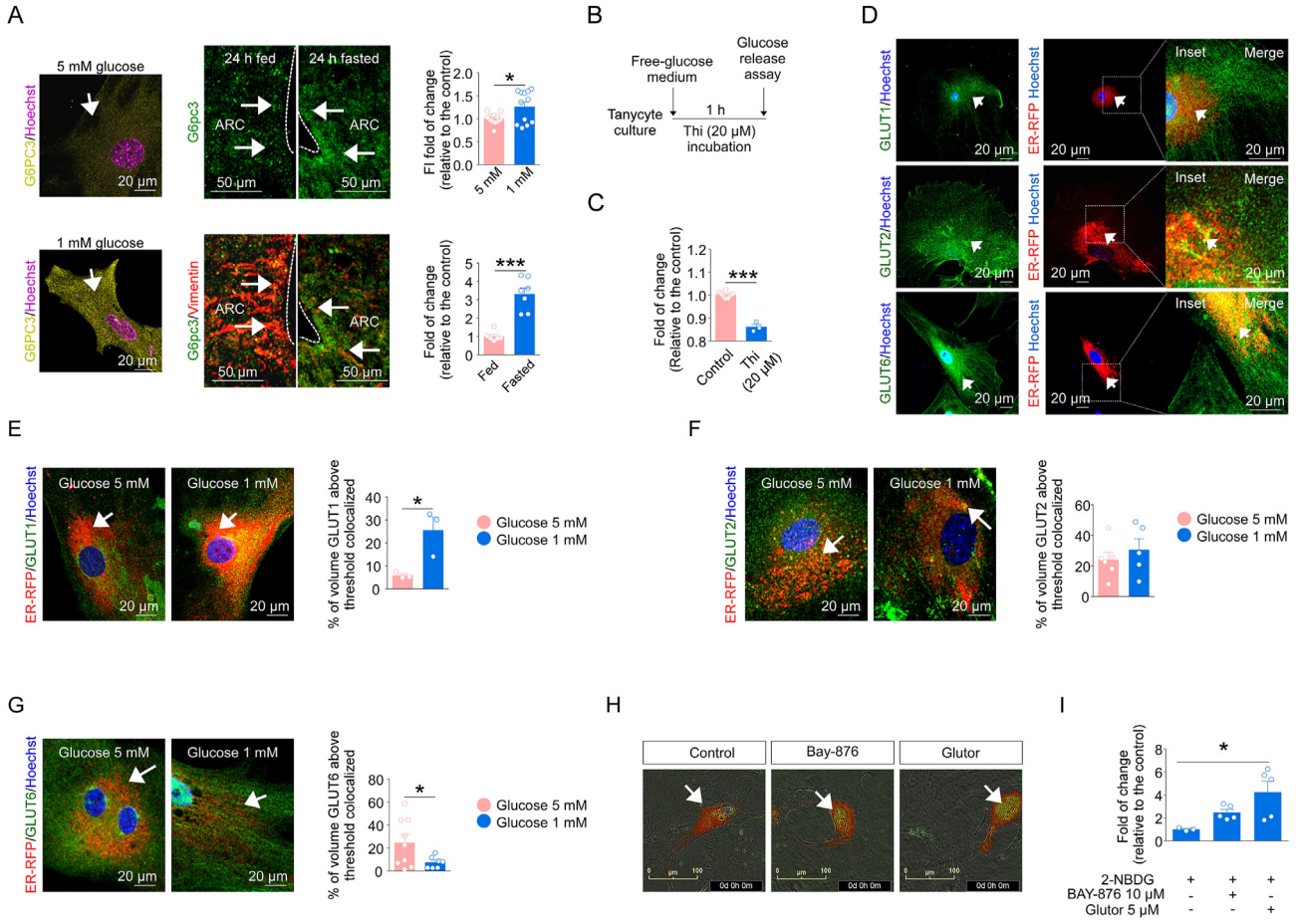

Figure 3: Tanycytes release glucose through GLUTs during hypoglycaemia. A. Immunolocalization of G6pc3 in tanycytes incubated for 24 h with 5 mM and 1 mM D-glucose. The graphs represent the fold-change in fluorescence intensity (FI) calculated for each treatment with respect to the 5 mM condition (n = 12 cells, three independent cultures). Immunolocalization of G6pc3 in fed (n = 6) and fasted (n = 7) mice. The graphs represent the fold change in fluorescence intensity (FI) calculated with respect to the fed condition. **B.** Experimental protocol to evaluate glucose release in tanycytes. **C.** Fold-changes in the extracellular glucose concentration of tanycyte cultures incubated for 2 h with glucose-free medium in the presence or absence of Thi (20 µM) (n = 3–8 independent cultures). **D.** Immunolocalization of GLUT1, GLUT2, and GLUT6 (green) in tanycytes transduced with the ER-RFP baculovirus (red). **E-G.** GLUT1 (J), GLUT2 (K), and GLUT6 (L) immunolocalization in tanycytes transduced with the ER-RFP baculovirus (n = 3–9 cells, three independent cultures). Cultures were incubated for 24 h with 1 and 5 mM D-glucose. For each condition, the percentage (%) of volume above threshold colocalized for GLUT1, GLUT2, and GLUT6 with the ER-RFP marker was calculated with respect to the control (Glucose 5 mM). **H.** Live-cell microscopy images. Tanycytes transduced with ER-RFP (red) and incubated with 2-NBDG (green) in the presence or absence of BAY-876 (10 µM) or Glutor (5 µM) **I.** Fold-change of fluorescence intensity (FI) of imagen shown in N (n = 3–5 independent cultures). *Gapdh* was used as a housekeeping gene for qPCR analyses. Data are represented as the mean ± SEM. Comparisons between two groups were made using a *t* test. Comparisons between more than two groups were made using one-way ANOVA. *P < 0.005.

the expression of GLUT1, GLUT2, and GLUT6 using qRT–PCR and Western blotting and found that hypoglycaemia does not generate changes in the mRNA and protein expression of GLUT1, GLUT2, or GLUT6 (Supplementary Figure 6A-B) (Supplementary Figure 7A-C).

Recent evidence strongly suggests that the intracellular localization of GLUT1 and GLUT2 may change in response to the energy requirements of the cell [38,39]. Consistent with this evidence, we evaluated whether hypoglycaemia in tanycytes induces the mobilization of GLUT1, GLUT2, and GLUT6 to the ER-subcellular structures to promote glucose export from the ER to the extracellular environment. Tanycytes were transduced with the ER-RFP construct and incubated for 24 h with 5 mM glucose (control condition) or 1 mM glucose (hypoglycaemia condition). As shown in Figure 3E (arrow), hypoglycaemia generates a redistribution of GLUT1, which is mostly colocalized with the ER-RFP marker. Quantification of the percentage of total GLUT1 colocalized with the ER-RFP marker shows that incubation with 1 mM glucose significantly increases the localization of GLUT1 in the ER (Figure 3E, graph).

A different situation was observed when we analysed the cellular distribution of GLUT2 and GLUT6. We did not detect changes in the distribution or quantification of the percentage of total GLUT2 colocalized with the ER-RFP marker in response to hypoglycaemia (Figure 3F, arrow). In contrast to the GLUT1 observations, we detected that hypoglycaemia in tanycytes generated a delocalization of GLUT6 from the ER-subcellular structures (Figure 3G, arrow). Therefore, the results suggest that eventually glucose stored in the ER lumen could be exported from the ER to the extracellular environment by GLUT1 and/or GLUT2.

To evaluate this hypothesis, we performed an ER retention assay of 2-NBDG by live-cell microscopy. We initially incubated tanycytes with the pharmacological inhibitors, BAY-876 (selective inhibitor of GLUT1) or Glutor (selective inhibitor of GLUT1, GLUT2, and GLUT3) [40,41]. After 15 min, we evaluated the retention of 2-NBDG in the ER (Supplementary Figure 8). As observed in Figure 3H, small clusters of 2-NBDG were observed in the ER in the control condition. A similar cluster of 2-NBDG

 © 2024 The Authors. Published by Elsevier GmbH. This is an open access article under the CC BY-NC license (http://creativecommons.org/licenses/by-nc/4.0/).

was observed when we evaluated retention in the presence of the GLUT1 inhibitor, Bay-876. However, the pharmacological inhibitor, Glutor, generated greater retention of 2-NBDG inside the ER (Figure 3H, arrow). These results were confirmed when we analysed the change ratio of the IF of the green (2-NBDG) channel over the red (ER) channel (Figure 3I). Altogether, the evidence suggests that tanycytes use GLUT1 and GLUT2 together to export glucose from the ER. Since the ER of tanycytes is in contact with the processes of these glial cells (Supplementary Figure 9, arrow) and the processes make close contact with neuroendocrine neurons in the hypothalamus [42], it is tempting to speculate that they use the glucose transfer mechanism to communicate with neurons responsible for hypothalamic energy balance.

3.4. G6PT-expressing tanycytes regulate peripheral adiposity

Taking advantage of the fact that tanycytes play a fundamental role in the control of hypothalamic energy balance [12,36,43,44] and that it had never been demonstrated that tanycytes can release glucose in hypoglycaemic conditions, we analysed the role of the tanycyte-G6Pase system in energy balance and metabolism. We generated a knockdown model for the G6PT subunit by intracerebroventricular (i.c.v) injection of an adenovirus-associated virus that expresses a shRNA in the U6 promoter region. Two weeks post-transduction, using mCherry fluorescence detection and three-dimensional and immunofluorescence analysis, AAV_1-sh*G6pt*-mCherry generates specific transduction in vimentin-positive tanycytes (Figure 4A, arrow).

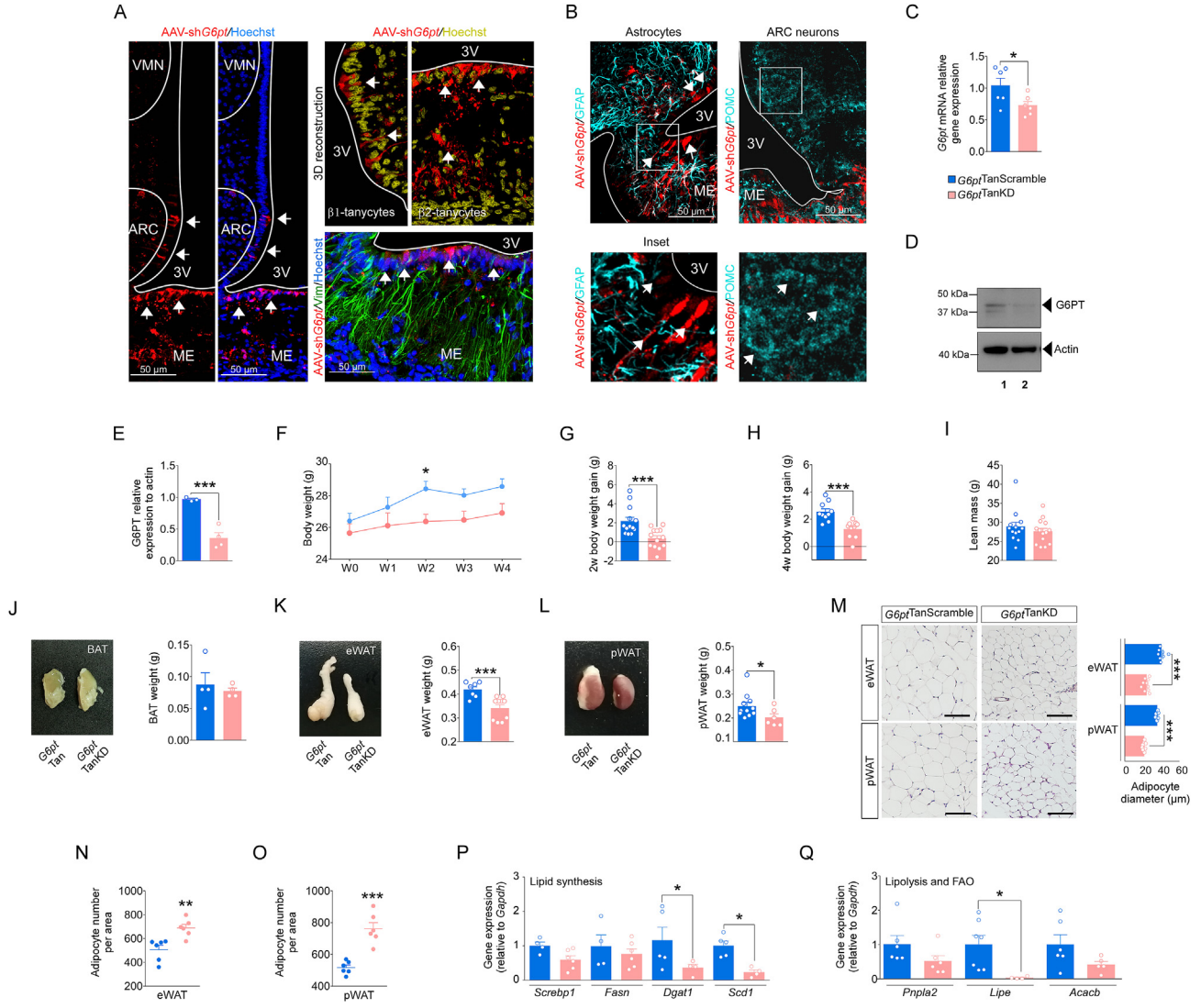

Figure 4: Selective *G6pt* deletion in tanycytes decreases adiposity. A. mCherry fluorescence (red) in coronal sections of transduced mice. 3D reconstruction was performed using Las X software. Immunolocalization of vimentin (green) in the basal hypothalamus of mice transduced with AAV_1-shG6pt-mCherry (red). **B.** Immunolocalization of GFAP (cyan) in the basal hypothalamus of mice transduced with AAV-sh*G6pt*-mCherry (red). **C.** *G6pt* mRNA expression levels in $G6pt^{TanScramble}$ (n = 6) or $G6pt^{TanKD}$ (n = 6) mice. **D.** Representative Western blot image for G6PT in $G6pt^{TanScramble}$ (Lane 1) or $G6pt^{TanKD}$ (Lane 2) mice. **E.** Densitometric quantification of the bands observed in D (n = 3–4 mice per condition). **F.** Body weight (g) in $G6pt^{TanScramble}$ (n = 12) or $G6pt^{TanKD}$ (n = 10) mice at 0, 1-, 2-, 3-, and 4-weeks post-transduction. **G.** BW gain in $G6pt^{TanScramble}$ (n = 13) or $G6pt^{TanKD}$ (n = 13) mice at 2 weeks post-transduction. **H.** BW gain in $G6pt^{TanScramble}$ (n = 10) or $G6pt^{TanKD}$ (n = 10) mice at 4 weeks post-transduction. **I.** Lean mass (g) in $G6pt^{TanScramble}$ (n = 13) or $G6pt^{TanKD}$ (n = 14) mice at 4 weeks post-transduction. **J-L.** BAT (J), eWAT (K), and pWAT (L) weight (g) in $G6pt^{TanScramble}$ (n = 4–12) or $G6pt^{TanKD}$ (n = 4–7) mice. **M.** Haematoxylin and eosin staining of eWAT and pWAT. **N–O.** Adipocyte number per area in eWAT and pWAT (n = 6 mice per condition). **P-Q.** mRNA expression levels of lipolysis-, lipogenesis-, and FAO-related genes in eWAT tissue from $G6pt^{TanScramble}$ (n = 4–7) or $G6pt^{TanKD}$ mice (n = 4–6). Data are represented as the mean ± SEM. Comparisons between two groups were made using an unpaired t test. Comparisons between two variables were made using one-way and two-way ANOVA. *P < 0.05, **P < 0.01; ***P < 0.001.

 © 2024 The Authors. Published by Elsevier GmbH. This is an open access article under the CC BY-NC license (http://creativecommons.org/licenses/by-nc/4.0/).

Additionally, AAV_1-sh*G6pt*-mCherry used did not transduce other glial cells located in the hypothalamus, such as astrocytes (Figure 4B, arrow). In addition, we determined that AAV_1-shG6pt-mCherry significantly decreased the mRNA and protein levels of G6PT (Figure 4C—E, Supplementary Figure 7D). It is important to mention that AAV_1-shG6pt-mCherry does not transduce glial cells located in other circumventricular organs, such as the vascular organ of the lamina terminalis (OVLT), the subfornical organ (SFO), the subcommissural organ (SCO), and the area postrema (AP) (Supplementary Figure 10A-D).

Next, we analysed the metabolic phenotype of G6PT subunit knockdown mice ($G6pt^{TanKD}$). We initially measured BW from the day of i.c.v. injection to 4 weeks post-transduction. As shown in Figure 4F, $G6pt^{TanKD}$ mice showed a significant decrease in BW at 2 weeks post-transduction. The decrease in BW persisted until 4 weeks post-transduction. Compared to control mice ($G6pt^{TanScramble}$), $G6pt^{TanKD}$ mice had a significantly lower BW gain at 2- and 4-weeks post-transduction (Figure 4G—H) that cannot be attributed to either a loss of lean mass or brown adipose tissue (BAT) (Figure 4I—J). However, $G6pt^{TanKD}$ mice had smaller epididymal (eWAT) and perirenal (pWAT) white adipose tissue (WAT) pads than $G6pt^{TanScramble}$ mice (Figure 4K-L). To determine if this phenomenon was associated with the decreased BW, we histologically analysed adipose tissue. Small adipocytes were observed in the eWAT and pWAT of $G6pt^{TanKD}$ mice (Figure 4M). Additionally, quantification of the number of adipocytes showed that $G6pt^{TanKD}$ mice had more adipocytes per field than $G6pt^{TanScramble}$ mice, suggesting a decrease in fat accumulation in $G6pt^{TanKD}$ mice (Figure 4N-O). To determine if the decrease in fat accumulation was due to a decrease in lipogenesis or an increase in lipolysis, we evaluated the mRNA expression levels of genes involved in both processes. We found a significant decrease in mRNA expression levels of *Dgta1*, an important regulator of triglyceride synthesis and lipid droplet formation in adipocytes [45] in $G6pt^{TanKD}$ mice (Figure 4P). Additionally, we found a significant decrease in the mRNA expression levels of *Scd1*, a catalyst for the synthesis of monounsaturated fatty acids (MUFAs) [46] (Figure 4P). Altogether, the results suggest that the silencing of *G6pt* in tanycytes may decrease the synthesis and storage of lipids. It is important to mention that $G6pt^{TanKD}$ mice also exhibited a reduction in the expression levels of the gene associated with lipolysis, *Lipe*, but we did not detect significant changes in the gene associated with FAO, *Acacb* (Figure 4Q).

3.5. *G6pt* silencing decreases food intake in response to fasting

To determine the cause of the reduction in adiposity, we first evaluated the basal food intake in $G6pt^{TanKD}$ and $G6pt^{TanScramble}$ mice for 24 h (Figure 5A) and found that $G6pt^{TanKD}$ mice had a basal food intake similar to mice $G6pt^{TanScramble}$ mice at 24 h (Figure 5B). Previous studies suggest that tanycytes regulate feeding behaviour mainly during food consumption at night [36]. To determine if *G6pt* silencing affects evening food consumption, we evaluated the amount of food consumed at night (12 h of darkness) and during the day (12 h of light). As shown in Figure 5C, *G6pt* silencing does not affect food intake in the dark phase or light phase of feeding. Previous studies have shown that tanycytes regulate meal initiation [36,43]; therefore, we evaluated whether *G6pt* silencing affects food intake during the first and second

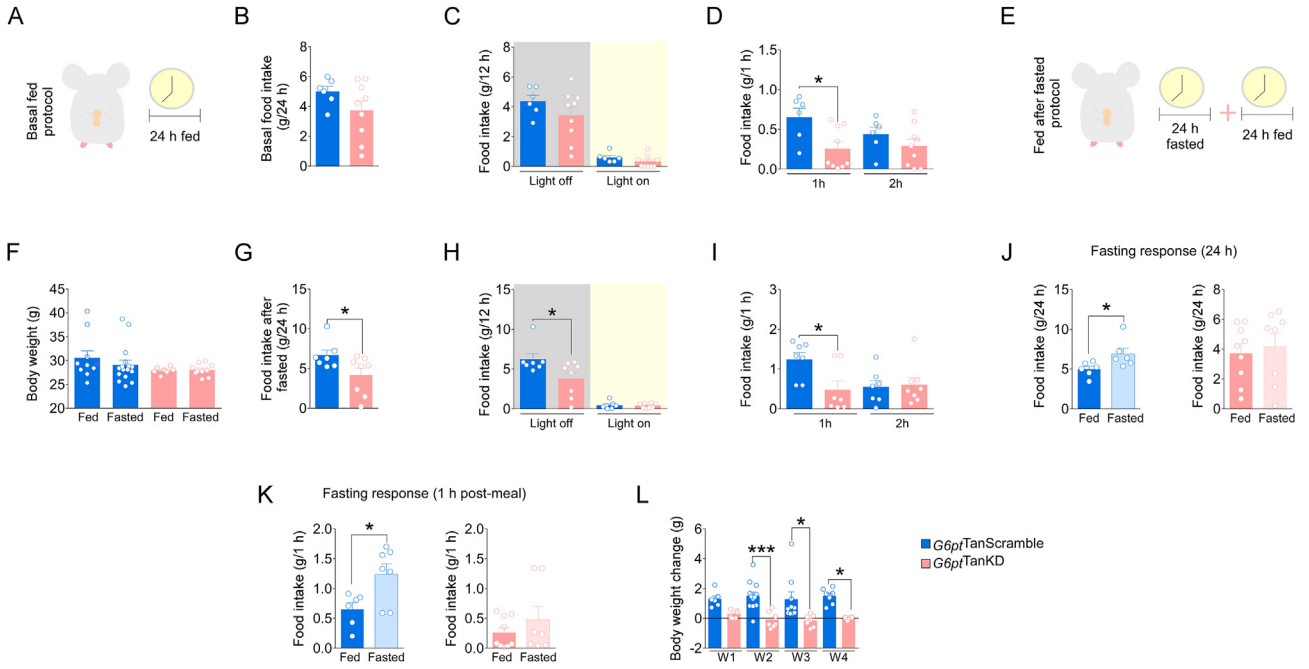

Figure 5: *G6pt* silencing decreased food intake in response to fasting. A. Basal food consumption protocol. **B.** Basal food intake in 24 h (g/24 h) by $G6pt^{TanScramble}$ (n = 6) or $G6pt^{TanKD}$ (n = 9) mice. **C.** Basal food consumption (g/12 h) by $G6pt^{TanScramble}$ (n = 6) or $G6pt^{TanKD}$ (n = 9) mice during the light-off and light-on phases. **D.** Basal food consumption (g/1 h) by $G6pt^{TanScramble}$ (n = 6) or $G6pt^{TanKD}$ (n = 9) mice during the first hour (1 h) and second hour (2 h) of the light-off phase. **E.** Food consumption after fasted protocol. **F.** BW in $G6pt^{TanScramble}$ (n = 10—16) and $G6pt^{TanKD}$ (n = 7—10) mice after the fed and fasted period. **G.** Food consumption in 24 h (g/24 h) by $G6pt^{TanScramble}$ (n = 7) or $G6pt^{TanKD}$ (n = 8) mice in response to 24 h of fasting. **H.** Food consumption (g/12 h) by $G6pt^{TanScramble}$ (n = 7) or $G6pt^{TanKD}$ (n = 8) mice during the light-off and light-on phases after 24 h of fasting. **I.** Food consumption (g/1 h) by $G6pt^{TanScramble}$ (n = 7) or $G6pt^{TanKD}$ (n = 7—8) mice during the first hour (1 h) and second hour (2 h) of the light-off phase after 24 h of fasting. **J.** Food consumption in 24 h (g/24 h) by $G6pt^{TanScramble}$ (n = 6) or $G6pt^{TanKD}$ (n = 8—9) mice in response to fed or 24 h of fasting. **K.** Food consumption in 1 h (g/1 h) by $G6pt^{TanScramble}$ (n = 6—7) or $G6pt^{TanKD}$ (n = 7—9) mice in response to 24 h of fasting. **L.** Body weight change (g) evaluated in $G6pt^{TanScramble}$ (n = 5—12) and $G6pt^{TanKD}$ (n = 5—10) for 4 weeks posttransduction. Data are represented as the mean ± SEM. Comparisons between two groups were made using an unpaired t test. Comparisons between two variables were made using one-way and two-way ANOVA. *P < 0.05.

 © 2024 The Authors. Published by Elsevier GmbH. This is an open access article under the CC BY-NC license (http://creativecommons.org/licenses/by-nc/4.0/).

hour after food presentation. *G6pt*^{TanKD} mice had significantly lower food intake during the first hour after food presentation (Figure 5D). These findings suggest that tanycytes expressing *G6pt* regulate meal initiation.

Following the analysis of food intake under basal conditions, we evaluated food intake in the dark and light phase in response to 24 h of fasting (Figure 5E). It is important to mention that the BW of *G6pt*^{TanScramble} and *G6pt*^{TanKD} mice did not change significantly in response to a 24 h of fasting (Figure 5F). *G6pt*^{TanKD} mice ate significantly less than *G6pt*^{TanScramble} mice in response to 24 h of fasting (Figure 5G). Additionally, *G6pt* silencing generated a significant decrease in dark-phase food consumption but did not affect feeding during the day (Figure 5H). These findings suggest that *G6pt* silencing affects total food intake consumption and the circadian rhythm regulation of feeding in response to fasting.

Previously, we demonstrated that the silencing of *G6pt* results in a reduction in food intake during the first hour of feeding. Consistent with this finding, we assessed food intake during the first and second hours of feeding in response to fasting. As shown in Figure 5I, *G6pt*^{TanScramble} mice responded to fasting by increasing food intake during the first hour after food presentation. However, no fasting response was observed in *G6pt*^{TanKD} mice, with a similar food intake during the first and second hours after food presentation (Figure 5I). To corroborate the loss in fasting response observed in *G6pt*^{TanKD} mice, we compared cumulative food intake at 24 h and 1 h post-feeding in fasted and ad libitum fed mice. As seen in Figure 5J, fasted *G6pt*^{TanScramble} mice exhibited significantly higher 24 h food intake compared to regularly fed *G6pt*^{TanScramble} mice (Figure 5J, purple bars). Interestingly, *G6pt*^{TanKD} mice did not increase their food intake in response to fasting, displaying a food intake similar to regularly fed *G6pt*^{TanKD} mice (Figure 5J, pink bars). It is worth noting that the loss of fasting response in *G6pt*^{TanKD} mice was also observed when assessing food intake after 1 h post-meal (Figure 5K). It is important to mention that the loss of response to fasting prior to the feeding phase may be the cause of the *G6pt*^{TanKD} mice presenting a lower weekly body weight gain compared to *G6pt*^{TanScramble} mice (Figure 5L). Overall, the data strongly suggest that tanycytes expressing *G6pt* are necessary to stimulate feeding and regulate meal initiation in response to prolonged fasting.

3.6. *G6pt* silencing decreases c-Fos and the *Npy* expression in response to fasting

Silencing of *G6pt* in tanycytes results in a decrease in food intake in response to fasting (Figure 5). To determine if this metabolic disruption is associated with alterations in glucose metabolism and/or pancreatic function, we analysed pre- and postprandial blood glucose levels. As shown in Figure 6A–B, *G6pt* silencing in tanycytes does not alter blood glucose levels in response to fasting or feeding (Figure 6A–B). Additionally, *G6pt*^{TanKD} mice do not develop glucose intolerance (Figure 6C) and exhibit blood insulin and glucagon levels similar to those of *G6pt*^{TanScramble} mice (Figure 6D–E). Thus, silencing of *G6pt* in tanycytes does not affect glucose metabolism.

Studies have shown that tanycytes can regulate the activity of neurons located in the ARC [12,36,43,44]. In this context, we evaluated whether the energy imbalance observed in *G6pt*^{TanKD} mice is associated with dysfunction in ARC neurons by quantifying the expression of c-Fos and neuropeptides synthesized in the ARC, such as *Npy* and *Pomc*, in response to 24 h of feeding or fasting. As shown in Figure 7A, no significant differences were observed between the *G6pt*^{TanScramble} and *G6pt*^{TanKD} mice in response to 24 h of feeding (Figure 7A). However, silencing *G6pt* in tanycytes results in a significant decrease in the number of c-Fos-positive cells in response to fasting (Figure 7B). These findings suggest that *G6pt* silencing in tanycytes leads to dysfunction in the hypothalamic ARC region, an alteration observed only in response to food deprivation.

The hypothalamic ARC is composed of orexigenic and anorexigenic neurons, such as *Npy* and *Pomc*, respectively. To identify which population is affected in response to *G6pt* silencing, we analysed *Npy* and *Pomc* mRNA expression levels during the fast-to-fed transition. As expected, *Npy* expression levels in *G6pt*^{TanScramble} mice were increased in response to 24 h of fasting and decreased in the fed

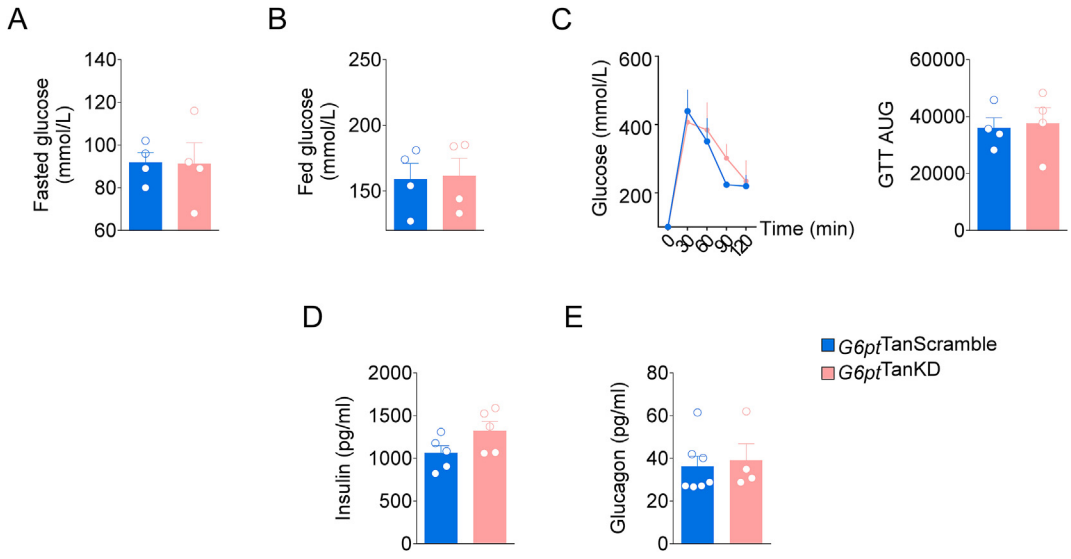

Figure 6: Selective *G6pt* deletion in tanycytes does not alter glucose metabolism. **A**. Blood glucose levels (mmol/l) in *G6pt*^{TanScramble} (n = 4) and *G6pt*^{TanKD} (n = 4) mice at the end of a 24 h fasting period. **B.** Blood glucose levels (mmol/l) in *G6pt*^{TanScramble} (n = 4) and *G6pt*^{TanKD} (n = 4) mice at the end of a 24 h fed period. **C.** Glucose tolerance test (GTT) in *G6pt*^{TanScramble} (n = 4) and *G6pt*^{TanKD} (n = 4) mice. **D.** Blood insulin levels in *G6pt*^{TanScramble} (n = 5) and *G6pt*^{TanKD} (n = 5) mice at the end of a 24 h fed period. **E.** Blood glucagon levels in *G6pt*^{TanScramble} (n = 7) and *G6pt*^{TanKD} (n = 4) mice at the end of a 24 h fed period. Data are represented as the mean ± SEM. Comparisons between two groups were made using an unpaired *t* test. Comparisons between two variables were made using one-way and two-way ANOVA.

 © 2024 The Authors. Published by Elsevier GmbH. This is an open access article under the CC BY-NC license (http://creativecommons.org/licenses/by-nc/4.0/).

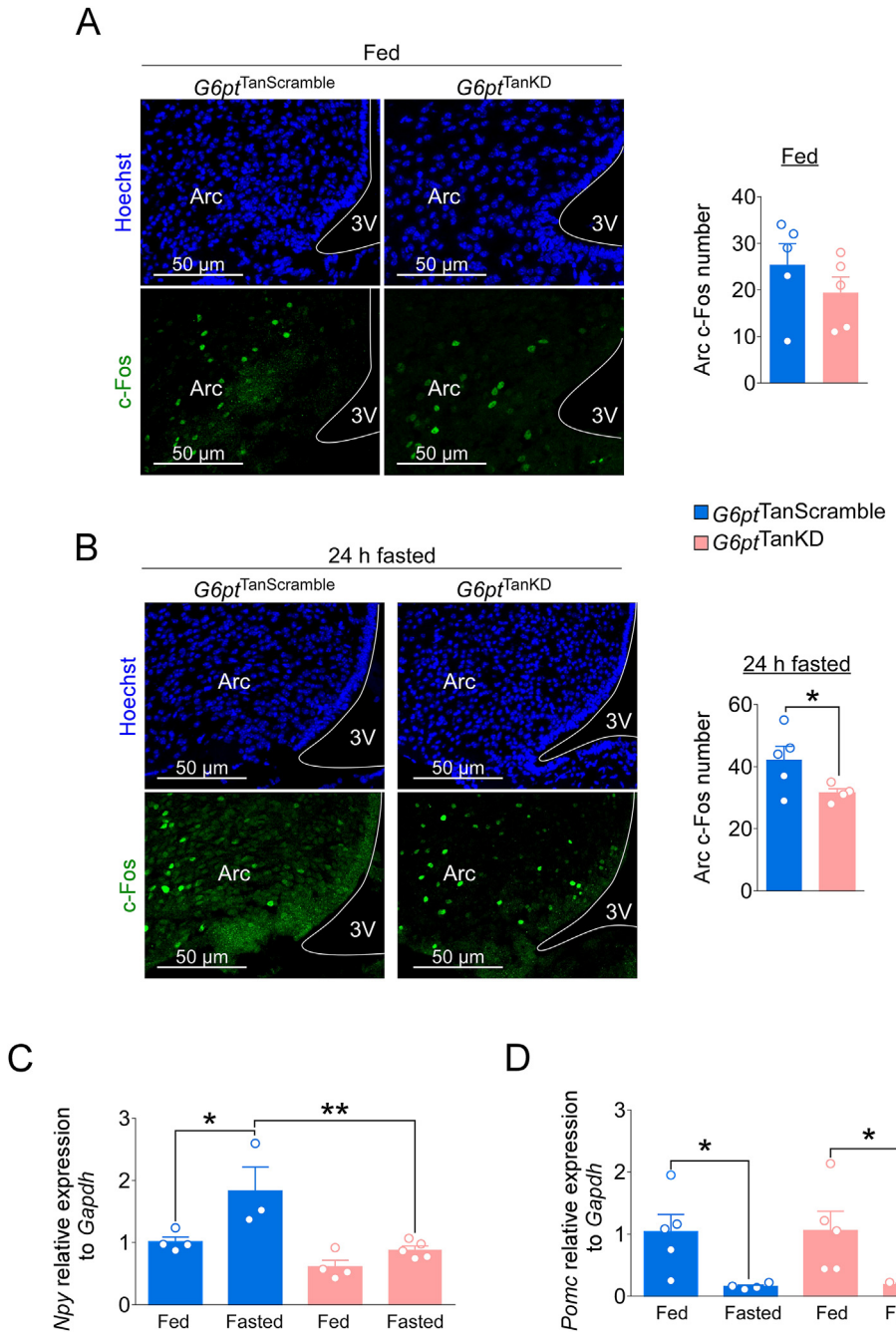

Figure 7: *G6pt* silencing decreased c-Fos and *Npy* expression in response to fasting. **A**. C-Fos immunolocalization and quantification of c-Fos-positive cells (green) in the ARC region of *G6pt*^{TanScramble} (blue bar) and *G6pt*^{TanKD} (pink bar) mice after 24 h of feeding (n = 5 mice per condition). **B.** C-Fos immunolocalization and quantification of c-Fos-positive cells in the ARC region of *G6pt*^{TanScramble} (blue bar) and *G6pt*^{TanKD} (pink bar) mice after 24 h of fasting (n = 4–5 mice per condition). **C.** *Npy* mRNA expression in basal fed and 24 h fasted *G6pt*^{TanScramble} (blue bar) or *G6pt*^{TanKD} (pink bar) mice (n = 4–5 mice per condition). **D.** *Pomc* mRNA expression in basal fed and 24 h fasted *G6pt*^{TanScramble} (blue bar) or *G6pt*^{TanKD} (pink bar) mice (n = 4–5 mice per condition). Hoechst was used as a nuclear marker. Data is represented as the mean ± SEM. Comparisons between two groups were made using an unpaired t-test. Comparisons between two variables were made using a two-way ANOVA test. *P < 0.05, **P < 0.01.

condition. However, fasting does not increase *Npy* expression levels in *G6pt*^{TanKD}, which remain constant during the fasting–refeeding transition (Figure 7C). A different scenario was observed when we evaluated the expression levels of the anorexigenic neuropeptide, *Pomc*. In this context, we detected that both *G6pt*^{TanScramble} and *G6pt*^{TanKD} mice maintained high levels of *Pomc mRNA* expression during feeding, which significantly decreased in response to 24 h of fasting (Figure 7D). Together, the data suggest that *G6pt* expression in tanycytes is required to stimulate *Npy* expression levels and promote feeding behaviour in response to fasting.

4. DISCUSSION

Since it was first proposed that tanycytes are glucose-sensing cells that possess a protein machinery similar to that of pancreatic beta cells, the scientific community has shown great interest in studying the

 © 2024 The Authors. Published by Elsevier GmbH. This is an open access article under the CC BY-NC license (http://creativecommons.org/licenses/by-nc/4.0/).

regulatory signals that tanycytes send to neurons in response to hyperglycaemia [12,36,43,44,47]. However, the regulatory signals that tanycytes send during hypoglycaemia have been poorly studied, and the mechanisms behind this physiological response are completely unknown. In this study, we show that tanycytes use the G6pase system and GLUTs to promote glucose release during hypoglycaemia, a signal that is necessary to stimulate food intake, possibly via activation of NPY neurons. In the CNS, the expression of the G6Pase system has been reported exclusively in foetal human astrocytes and in mouse astrocytes [7,9,10]. Both astrocytes and tanycytes express the G6PT subunit and the G6pc3 catalytic subunit, unlike hepatocytes, which express the G6pc1 catalytic subunit [48–50]. It is important to mention that the G6pc3 phosphatase is homologous to the G6pc1 phosphatase, and both proteins project their catalytic site toward the reticular lumen and hydrolyse G6P with similar *Km* values [51]. Therefore, tanycytes share similar properties with hepatocytes regarding G6P hydrolysis.

Surprisingly, our data show that tanycytes sequester G6P in the ER and that this phenomenon depends on the activity of both G6PT and G6pc3 phosphatases. Decreased G6PT activity (induced by incubation with CHA) resulted in lower G6P uptake. These findings support the substrate-transporter model proposed by Arion and colleagues, which suggests that the incorporation of G6P into the reticular lumen is mediated by a G6PT [2]. While the effect of decreased joint activity of G6PT and G6pc3 on G6P sequestration has never been shown in the literature, it has been reported that there is a decrease in G6P sequestration when *G6pc3* phosphatase is silenced [9,52,53]. Consistent with this notion, silencing *G6pc3* in astrocytes leads to a decrease in reticular G6P uptake, ATP production, and reticular Ca^{2+} uptake [9]. In this scenario, we propose the following model to explain the glucose sequestration process. Due to the privileged location of tanycytes in the 3V [13,14] and the apical expression of low-affinity, high-capacity glucose transporters, such as GLUT2 and GLUT6 [12,36,37], tanycytes in normal or hyperglycaemic conditions can directly incorporate glucose from the CSF (Figure 8A). Intracellularly, glucose can be phosphorylated to G6P by the enzyme glucokinase [43]. Cytosolic G6P can participate in two parallel and independent pathways: (1) G6P can enter the glycolytic pathway to generate lactate and promote feeding cessation through the activation of POMC neurons, as recently reported [44] and (2) it can enter the reticular lumen using the G6Pase system (Figure 8A). In the latter pathway, the ER could act as an intracellular glucose reservoir, which is replenished

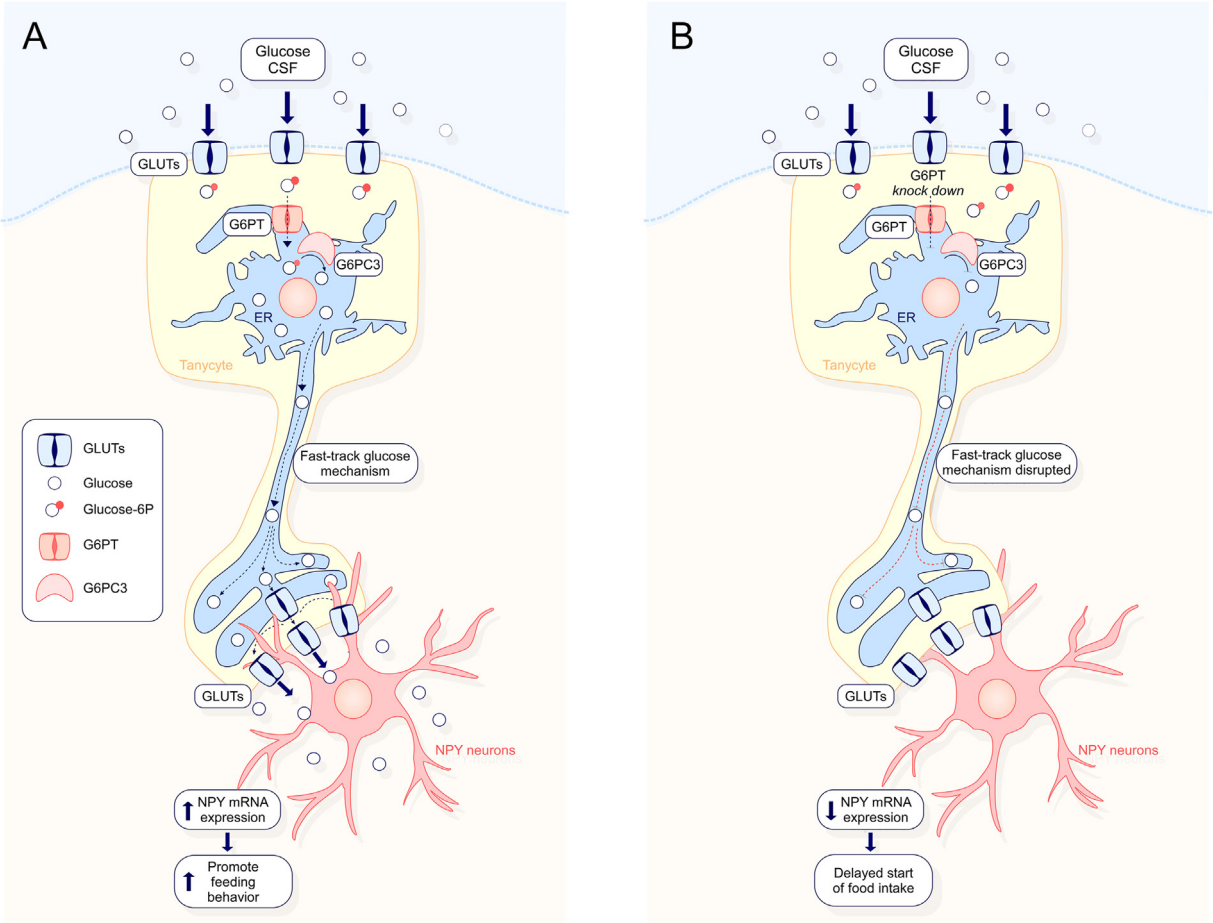

Figure 8: The G6Pase system in tanycytes and its role in the control of food intake. A. Under normo- or hyperglycaemic conditions, tanycytes can incorporate glucose via GLUT2 and GLUT6 from the CSF into the intracellular environment. Once inside, glucose can be phosphorylated to G6P by the enzyme glucokinase and sequestered into the reticular lumen by the action of the G6PT. G6P in the reticular lumen is hydrolysed by G6PC3 phosphatase, resulting in the formation of free glucose [2]. Glucose in the ER can travel several microns until it encounters GLUT1, which facilitates its release from the ER lumen into the extracellular space. The glucose released during hypoglycaemia into the hypothalamic parenchyma is necessary to promote the synthesis of NPY and stimulate food intake. **B.** When the G6P transporter is silenced, the uptake of reticular G6P decreases, disrupting the mechanism of rapid glucose release during hypoglycaemia. The decrease in glucose release directly impacts NPY neurons, causing a delay in the onset of feeding.

 © 2024 The Authors. Published by Elsevier GmbH. This is an open access article under the CC BY-NC license (http://creativecommons.org/licenses/by-nc/4.0/).

during hyperglycaemia and added to the glycogen stores that these glial cells possess [13,54]. Now, in this scenario, an intriguing question arises. Why do tanycytes store glucose in the ER? Our data suggest that tanycytes use the glucose stored in the ER to transfer it to NPY neurons during hypoglycaemia (Figure 8A). Previously, it has been reported that 40% of NPY neurons are glucose-inhibited neurons, which remain depolarized when glucose concentrations range from 0.1 mM to 2.5 mM [55,56]. Taking advantage of the fact that tanycytes can transfer glucose to the ARC during hypoglycaemia [35] and that hypothalamic neurons express the high-affinity, low-capacity glucose transporter, GLUT3 [57], it is tempting to speculate that tanycytes may use reticular glucose reservoirs to maintain glucose concentrations in the hypothalamic parenchyma within the range of activation of NPY neurons. Since glycogen breakdown during hypoglycaemia is a process that can take minutes or even hours [58], we propose that tanycytes use this mechanism for rapid transfer of glucose to the hypothalamic parenchyma, overcoming the need for glycogen to mediate this response. Nevertheless, while our current data suggest a potential link, indicating that tanycytes might utilize the glucose reservoir in the ER to facilitate its transfer to NPY neurons during episodes of hypoglycemia, it is crucial to acknowledge the need for further experiments to substantiate and validate this hypothesis.

Surprisingly, we determined that tanycytes export glucose from the ER via GLUTs. Since it has been shown in permeabilized cells that glucose does not readily enter the reticular lumen [9], it is possible that the glucose transporters found in the ER, such as GLUT1 and GLUT2, can exclusively export glucose from the ER to the extracellular space. Here, we demonstrate that GLUT1 and GLUT6 undergo redistribution in response to hypoglycaemia in tanycytes. In line with this evidence, recent studies suggest that GLUT1 can translocate in response to decreases in intracellular ATP concentration [39]. However, further studies are needed to analyse the translocation of both GLUT1 and GLUT6 in response to hypoglycaemia.

The ER of tanycytes is elongated and projects along the processes of glial cells, which have been shown to establish close contact with ARC neurons. The proximity between both cell membranes can promote the transfer of glucose from the ER membranes to the plasma membrane and from there to the hypothalamic parenchyma. In this way, glucose can travel from the CSF to the hypothalamic parenchyma through an intracellular pathway that protects glucose from entering metabolic pathways, such as glycolysis and the pentose phosphate pathway. Since GLUT1 is preferentially located in the processes of tanycytes *in vivo*, it is feasible to propose that glucose is released into the hypothalamic parenchyma through this transporter, as recently described [35].

In this study, we determined that *in vivo* silencing of the G6Pase system generates deficient fat accumulation in WAT tissue associated with a decrease in lipogenic genes. Recently, several authors have reported on the role of tanycytes in the control of adiposity [15,16,43,47,59]. In this context, $G6pt^{TanKD}$ mice developed a tanycyte metabolic phenotype similar to that observed in the FGF21 knock-out mouse. In these mice, tanycytes promote lipid mobilization, increasing energy expenditure and decreasing fat accumulation [15]. Intriguingly, we detected a decrease in the expression level of the gene associated with lipolysis, *Lipe,* in $G6pt^{TanKD}$ mice. We believe that the decrease in the expression of this gene may be a compensatory effect aimed at limiting the release of fatty acids from adipocytes and thus having substrates for the synthesis of cell membranes.

In the present study, *G6pt* silencing generates a decrease in food intake under prolonged fasting conditions, a response that is strictly associated with a decrease in *Npy* levels but not *Pomc* levels. Currently, it has been reported that tanycytes release lactate to POMC neurons to trigger cessation of feeding [44]. However, this is a response that is generated in hyperglycaemia. Based on our background, we propose that in hypoglycaemia, tanycytes promote food intake by modulating the rapid transfer of glucose to NPY neurons. Since we have determined that G6pt silencing alters food intake in fed and fasted mice, we believe that this mechanism may be immediately activated in response to decreases in glucose concentration that precede feeding. The disruption in G6P sequestration may result in reduced glucose transfer to NPY neurons, resulting in diminished Npy release and decreased stimulation of food intake (Figure 8B). Finally, the results presented in this study highlight the critical role of G6Pase-expressing tanycytes in regulating energy homeostasis in the brain and could have potential therapeutic implications in the treatment of metabolic diseases and appetite disorders.

FUNDING

The work was supported by grants from the Agencia Nacional de Investigación y Desarrollo-ANID: "Fondecyt de postdoctorado" N°3210076 (to M.J.B), "Fondecyt de iniciación" N°11200335 (to L.F), "Fondecyt regular" N° 1221147 (to F.N) and VIU N° 22P0021 (to M.V), "Fondecyt de iniciación" N°11240089 (to M.J.B).

DISCLOSURE STATEMENT

The authors declare no competing interests.

CREDIT AUTHORSHIP CONTRIBUTION STATEMENT

María José Barahona: Writing — original draft, Methodology, Investigation, Formal analysis, Data curation, Conceptualization. **Luciano Ferrada:** Writing — review & editing, Methodology, Formal analysis. **Matías Vera:** Formal analysis. **Francisco Nualart:** Writing — review & editing, Supervision, Project administration, Methodology, Investigation, Data curation, Conceptualization.

DECLARATION OF COMPETING INTEREST

The authors declare that there are no conflict of interests.

DATA AVAILABILITY

Data will be made available on request.

APPENDIX A. SUPPLEMENTARY DATA

Supplementary data to this article can be found online at https://doi.org/10.1016/j.molmet.2024.101940.

REFERENCES

[1] Arion WJ, Nordlie RC. Liver glucose-6-phosphatase and pyrophosphate-glucose phosphotransferase: effects of fasting. Biochem Biophys Res Commun 1965;20(5):606—10.

[2] Arion WJ, Wallin BK, Lange AJ, Ballas LM. On the involvement of a glucose 6-phosphate transport system in the function of microsomal glucose 6-phosphatase. Mol Cell Biochem 1975;6:75—83. https://doi.org/10.1007/BF01732001.

 © 2024 The Authors. Published by Elsevier GmbH. This is an open access article under the CC BY-NC license (http://creativecommons.org/licenses/by-nc/4.0/).

[3] van Schaftingen E, Gerin I. The glucose-6-phosphatase system. Biochem J 2002;362(Pt 3):513–32.
[4] Cori GT, Cori CF. Glucose-6-phosphatase of the liver in glycogen storage disease. J Biol Chem 1952;199(2):661–7.
[5] de Duve C, Berthet J, Hers HG, Dupret L. Le systeme hexosephosphatasique. I. Existence d'une glucose-6-phosphatase specifique dans le foie. Bull. Soc. Chim. Biol. 1949;31:1242–53.
[6] Hers HG, Berthet J, Berthet L, de Duve C. *Le systeme hexosephosphatasique*. III. Localisation intra-cellulaire des ferments par centrifugation *fractionne*. Bull. Soc. Chim. Biol. 1951;33:21–41.
[7] Pellerin L. Neuroenergetics: astrocytes have a sweet spot for glucose. Curr Biol 2018;28(21):R1258–60.
[8] Hers HG, Berthet J, Berthet L, De Duve C. [The hexose-phosphatase system. III. Intracellular localization of enzymes by fractional centrifugation]. Bull Soc Chim Biol (Paris) 1951;33:21–41.
[9] Muller MS, Fouyssac M, Taylor CW. Effective glucose uptake by human astrocytes requires its sequestration in the endoplasmic reticulum by glucose-6-phosphatase-beta. Curr Biol 2018;28(21):3481–3486 e4.
[10] Ghosh A, Cheung YY, Mansfield BC, Chou JY. Brain contains a functional glucose-6-phosphatase complex capable of endogenous glucose production. J Biol Chem 2005;280:11114–9. https://doi.org/10.1074/jbc.M410894200.
[11] Forsyth RJ, Bartlett K, Burchell A, Scott HM, Eyre JA. Astrocytic glucose-6-phosphatase and the permeability of brain microsomes to glucose 6-phosphate. Biochem J 1993;294(Pt 1):145–51. https://doi.org/10.1042/bj2940145.
[12] Barahona MJ, Llanos P, Recabal A, Escobar-Acuna K, Elizondo-Vega R, Salgado M, et al. Glial hypothalamic inhibition of GLUT2 expression alters satiety, impacting eating behavior. Glia 2018;66(3):592–605.
[13] Rodriguez EM, Blázquez JL, Pastor FE, Peláez B, Pena P, Peruzzo B, et al. Hypothalamic tanycytes: a key component of brain-endocrine interaction. Int Rev Cytol 2005;247:89–164.
[14] Rodriguez E, Rodriguez E, Guerra M, Peruzzo B, Blazquez JL. Tanycytes: a rich morphological history to underpin future molecular and physiological investigations. J Neuroendocrinol 2019;31(3):e12690.
[15] Geller S, Arribat Y, Netzahualcoyotzi C, Lagarrigue S, Carneiro L, Zhang L, et al. Tanycytes regulate lipid homeostasis by sensing free fatty acids and signaling to key hypothalamic neuronal populations via FGF21 secretion. Cell Metabol 2019;30(4):833–844 e7.
[16] Imbernon M, Saporano C, Cederberg Helms HC, Duquenne M, Fernandois D, Deligia E, et al. Tanycytes control hypothalamic liraglutide uptake and its anti-obesity actions. Cell Metabol 2022;34(7):1054–1063 e7.
[17] Langlet F. Targeting tanycytes: balance between efficiency and specificity. Neuroendocrinology 2020;110(7–8):574–81.
[18] Barahona MJ, Rojas J, Uribe EA, Garcia-Robles MA. Tympanic membrane rupture during stereotaxic surgery disturbs the normal feeding behavior in rats. Front Behav Neurosci 2020;14:591204.
[19] Prevot V, Dehouck B, Sharif A, Ciofi P, Giacobini P, Clasadonte J. The versatile tanycyte: a hypothalamic integrator of reproduction and energy metabolism. Endocr Rev 2018;39(3):333–68.
[20] Hutton JC, O'Brien RM. Glucose-6-phosphatase catalytic subunit gene family. J Biol Chem 2009;284(43):29241–5.
[21] Nordlie RC, Arion WJ. Evidence for the common identity of glucose 6-phosphatase, inorganic pyrophosphatase, and pyrophosphate-glucose phosphotransferase. J Biol Chem 1964;239:1680–5.
[22] Arion WJ, Ballas LM, Lange AJ, Wallin BK. Microsomal membrane permeability and the hepatic glucose-6-phosphatase system. Interactions of the system with D-mannose 6-phosphate and D-mannose. J Biol Chem 1976;251(16):4891–7.
[23] Zou C, Wang Y, Shen Z. 2-NBDG as a fluorescent indicator for direct glucose uptake measurement. J Biochem Biophys Methods 2005;64(3):207–15.
[24] Yamada K, Saito M, Matsuoka H, Inagaki N. A real-time method of imaging glucose uptake in single, living mammalian cells. Nat Protoc 2007;2(3):753–62.
[25] Marini C, Ravera S, Buschiazzo A, Bianchi G, Orengo AM, Bruno S, et al. Discovery of a novel glucose metabolism in cancer: the role of endoplasmic reticulum beyond glycolysis and pentose phosphate shunt. Sci Rep 2016;6:25092.
[26] Hemmerle H, Burger HJ, Below P, Schubert G, Rippel R, Schindler PW, et al. Chlorogenic acid and synthetic chlorogenic acid derivatives: novel inhibitors of hepatic glucose-6-phosphate translocase. J Med Chem 1997;40(2):137–45.
[27] Arion WJ, Canfield WK, Ramos FC, Schindler PW, Burger HJ, Hemmerle H, et al. Chlorogenic acid and hydroxynitrobenzaldehyde: new inhibitors of hepatic glucose 6-phosphatase. Arch Biochem Biophys 1997;339(2):315–22.
[28] Belkaid A, Currie JC, Desgagnes J, Annabi B. The chemopreventive properties of chlorogenic acid reveal a potential new role for the microsomal glucose-6-phosphate translocase in brain tumor progression. Cancer Cell Int 2006;6:7.
[29] Sakemi S, Hirai H, Ichiba H, Inagaki T, Kato Y, Kojima N, et al. Thielavins as glucose-6-phosphatase (G6Pase) inhibitors: producing strain, fermentation, isolation, structural elucidation and biological activities. J Antibiot (Tokyo) 2002;55(11):941–51.
[30] Khan A, Low H, Efendic S. Effects of fasting and refeeding on the activity of hepatic glucose-6-phosphatase in rats. Acta Physiol Scand 1985;124(4):591–6.
[31] Segal HL, Washko ME. Studies of liver glucose 6-phosphatase. III. Solubilization and properties of the enzyme from normal and diabetic rats. J Biol Chem 1959;234(8):1937–41.
[32] Xie W, Li Y, Mechin MC, Van De Werve G. Up-regulation of liver glucose-6-phosphatase in rats fed with a P(i)-deficient diet. Biochem J 1999;343(Pt 2):393–6.
[33] Takanaga H, Frommer WB. Facilitative plasma membrane transporters function during ER transit. Faseb J 2010;24(8):2849–58.
[34] Fehr M, Takanaga H, Ehrhardt DW, Frommer WB. Evidence for high-capacity bidirectional glucose transport across the endoplasmic reticulum membrane by genetically encoded fluorescence resonance energy transfer nanosensors. Mol Cell Biol 2005;25(24):11102–12.
[35] Rodriguez-Cortes B, Hurtado-Alvarado G, Martínez-Gómez R, León-Mercado LA, Prager-Khoutorsky M, Buijs RM. Suprachiasmatic nucleus-mediated glucose entry into the arcuate nucleus determines the daily rhythm in blood glycemia. Curr Biol 2022;32(4):796–805.e4.
[36] Barahona MJ, Langlet F, Labouèbe G, Croizier S, Picard A, Thorens B, et al. GLUT2 expression by glial fibrillary acidic protein-positive tanycytes is required for promoting feeding-response to fasting. Sci Rep 2022;12(1):17717.
[37] Martinez F, Cifuentes M, Tapia JC, Nualart F. The median eminence as the hypothalamic area involved in rapid transfer of glucose to the brain: functional and cellular mechanisms. J Mol Med (Berl) 2019;97(8):1085–97.
[38] Tsytkin-Kirschenzweig S, Cohen M, Nahmias Y. Tracking GLUT2 translocation by live-cell imaging. Methods Mol Biol 2018;1713:241–54.
[39] Mamun AA, Hayashi H, Yamamura A, Nayeem MJ, Sato M. Hypoxia induces the translocation of glucose transporter 1 to the plasma membrane in vascular endothelial cells. J Physiol Sci 2020;70(1):44.
[40] Siebeneicher H, Cleve A, Rehwinkel H, Neuhaus R, Heisler I, Müller T. Identification and optimization of the first highly selective GLUT1 inhibitor BAY-876. ChemMedChem 2016;11(20):2261–71.
[41] Reckzeh ES, Karageorgis G, Schwalfenberg M, Ceballos J, Nowacki J, Stroet MC, et al. Inhibition of glucose transporters and glutaminase synergistically impairs tumor cell growth. Cell Chem Biol 2019;26(9):1214–1228 e25.
[42] Pasquettaz R, Kolotuev I, Rohrbach A, Gouelle C, Pellerin L, Langlet F. Peculiar protrusions along tanycyte processes face diverse neural and nonneural cell types in the hypothalamic parenchyma. J Comp Neurol 2021;529:553–75. https://doi.org/10.1002/cne.24965.
[43] Rohrbach A, Caron E, Dali R, Brunner M, Pasquettaz R, Kolotue VI, et al. Ablation of glucokinase-expressing tanycytes impacts energy balance and increases adiposity in mice. Mol Metabol 2021;53:101311.

 © 2024 The Authors. Published by Elsevier GmbH. This is an open access article under the CC BY-NC license (http://creativecommons.org/licenses/by-nc/4.0/).

[44] Lhomme T, Clasadonte J, Imbernon M, Fernandois D, Sauve F, Caron E, et al. Tanycytic networks mediate energy balance by feeding lactate to glucose-insensitive POMC neurons. J Clin Invest 2021;131(18).
[45] Harris CA, Haas JT, Streeper RS, Stone SJ, Kumari M, Yang K, et al. DGAT enzymes are required for triacylglycerol synthesis and lipid droplets in adipocytes. J Lipid Res 2011;52(4):657–67.
[46] Ahmed AL, Syed DN, Ntambi JM. Insights into stearoyl-CoA desaturase-1 regulation of systemic metabolism. Trends Endocrinol Metabol 2017;28(12):831–42.
[47] Duquenne M, Folgueira C, Bourouh C, Millet M, Silva A, Clasadonte J, et al. Leptin brain entry via a tanycytic LepR-EGFR shuttle controls lipid metabolism and pancreas function. Nat Metab 2021;3(8):1071–90.
[48] Chou JY, Jun HS, Mansfield BC. Type I glycogen storage diseases: disorders of the glucose-6-phosphatase/glucose-6-phosphate transporter complexes. J Inherit Metab Dis 2015;38(3):511–9.
[49] La Rose M, Bazioti V, Hoogerland JA, Svendsen AF, Groenen AG, Van Faassen M, et al. Hepatocyte-specific glucose-6-phosphatase deficiency disturbs platelet aggregation and decreases blood monocytes upon fasting-induced hypoglycemia. Mol Metabol 2021;53:101265.
[50] Claxton DP, Overway EM, Oeser JK, O'Brien RM, McHaourab HS. Biophysical and functional properties of purified glucose-6-phosphatase catalytic subunit 1. J Biol Chem 2022;298(1):101520.
[51] Guionie O, Clottes E, Stafford K, Burchell A. Identification and characterisation of a new human glucose-6-phosphatase isoform. FEBS Lett 2003;551(1–3):159–64.
[52] Jun HS, Cheung YY, Lee YM, Mansfield BC, Chou JY. Glucose-6-phosphatase-beta, implicated in a congenital neutropenia syndrome, is essential for macrophage energy homeostasis and functionality. Blood 2012;119(17):4047–55.
[53] Jun HS, Lee YM, Cheung YY, McDermott DH, Murphy PM, De Ravin SS, et al. Lack of glucose recycling between endoplasmic reticulum and cytoplasm underlies cellular dysfunction in glucose-6-phosphatase-beta-deficient neutrophils in a congenital neutropenia syndrome. Blood 2010;116(15):2783–92.
[54] Nilaweera K, Herwig A, Bolborea M, Campbell G, Mayer CD, Morgan PJ, et al. Photoperiodic regulation of glycogen metabolism, glycolysis, and glutamine synthesis in tanycytes of the Siberian hamster suggests novel roles of tanycytes in hypothalamic function. Glia 2011;59(11):1695–705.
[55] Murphy BA, Fioramonti X, Jochnowitz N, Fakira K, Gagen K, Contie S, et al. Fasting enhances the response of arcuate neuropeptide Y-glucose-inhibited neurons to decreased extracellular glucose. Am J Physiol Cell Physiol 2009;296(4):C746–56.
[56] Hirschberg PR, Sarkar P, Teegala SB, Routh VH. Ventromedial hypothalamus glucose-inhibited neurones: a role in glucose and energy homeostasis? J Neuroendocrinol 2020;32(1):e12773.
[57] Yu S, Tooyama I, Ding WG, Kitasato H, Kimura H. Immunohistochemical localization of glucose transporters (GLUT1 and GLUT3) in the rat hypothalamus. Obes Res 1995;3(Suppl 5):753S–60S.
[58] Murray B, Rosenbloom C. Fundamentals of glycogen metabolism for coaches and athletes. Nutr Rev 2018;76(4):243–59.
[59] Yoo S, Cha D, Kim S, Jiang L, Cooke P, Adebesin M, et al. Tanycyte ablation in the arcuate nucleus and median eminence increases obesity susceptibility by increasing body fat content in male mice. Glia 2020;68(10):1987–2000.

 © 2024 The Authors. Published by Elsevier GmbH. This is an open access article under the CC BY-NC license (http://creativecommons.org/licenses/by-nc/4.0/).